Title: Glucose-oxygen deprivation constrains HMGCR function and Rac1 prenylation and activates the NLRP3 inflammasome

Authors: Nora Raulien[1,2]†, Kathleen Friedrich[1]†, Sarah Strobel[1], Stefanie Raps[1], Friederike Hecker[1], Matthias Pierer[1], Erik Schilling[1], Elke Lainka[3], Tilmann Kallinich[4], Sven Baumann[5], Katarina Fritz-Wallace[5], Ulrike Rolle-Kampczyk[5], Martin von Bergen[5,6,7], Achim Aigner[8], Alexander Ewe[8], Georg Schett[9,10], Michael Cross[11], Manuela Rossol[1,12]†, Ulf Wagner[1]†*

Affiliations:

[1] Division of Rheumatology, Department of Endocrinology, Nephrology, Rheumatology, Leipzig University; Leipzig, Germany.

[2] Institute of Anatomy, University Leipzig, Leipzig, Germany

[3] Department of Pediatric Gastroenterology, Hepatology and Liver Transplantation, University Children's Hospital Essen; Essen, Germany.

[4] Department of Pediatric Respiratory Medicine, Immunology and Critical Care Medicine, Charité Universitätsmedizin Berlin; Berlin, Germany.

[5] Department of Molecular Systems Biology, Helmholtz Centre for Environmental Research GmbH; Leipzig, Germany.

[6] Institute for Biochemistry, Faculty of Life Sciences, Leipzig University; Leipzig, Germany.

[7] German Centre for Integrative Biodiversity Research (iDiv) Halle-Jena-Leipzig; Leipzig, Germany.

[8] Rudolf-Boehm-Institute for Pharmacology and Toxicology, Clinical Pharmacology, Faculty of Medicine, Leipzig University, Leipzig, Germany.

[9] Department of Internal Medicine 3 - Rheumatology and Immunology, Friedrich-Alexander University (FAU) Erlangen-Nürnberg and Universitätsklinikum Erlangen, Erlangen, Germany.

[10] Deutsches Zentrum Immuntherapie, Friedrich-Alexander University (FAU) Erlangen-Nürnberg and Universitätsklinikum Erlangen, Erlangen, Germany.

[11] Leipzig Medical Center, Clinic for Hematology and Cell Therapy, University Clinic Leipzig; Leipzig, Germany.

[12] Molecular Immunology, Faculty of Health Sciences, Brandenburg Technische Universität Cottbus-Senftenberg, Germany

† These authors contributed equally to this work

*Corresponding author. Email: ulf.wagner@medizin.uni-leipzig.de

Abstract: Hypoxia and low glucose often occur simultaneously at sites of inflammation due to malperfusion, acidosis and upregulated glycolytic activity of monocytes. The link between such conditions and inflammation is unclear.

Here we show that concomitant glucose deprivation and hypoxia activate the NLRP3 inflammasome due to inhibition of the pentose phosphate pathway and constrained HMGCR function. Consequently, geranylgeranyl pyrophosphate synthesis is diminished, which leads to hypoprenylation of Rac1, increased binding of non-prenylated Rac1 to IQGAP1, and NLRP3 activation. In monocytes from patients with mevalonate kinase deficiency and Muckle-Wells syndrome, a compromised mevalonate pathway causes increased IL-1β release under restricted oxygen and glucose supply. We propose that this mechanism might also be active in inflammatory autoimmune conditions and can be alleviated by Rac1 inhibitors such as thiopurines.

One-Sentence Summary: Compromised blood supply triggers NLRP3 inflammasome assembly due to suppressed HMGCR expression and hypoprenylation of Rac1.

Main Text:

INTRODUCTION

At sites of inflammation and infection, restricted perfusion leads to hypoxia and impaired nutrient supply (*1*). Immune cells at such sites, both of the lymphoid and myeloid lineage, switch their metabolism to glycolysis and increase glucose consumption (*2–7*), further reducing the local glucose concentration.

In monocytes, such conditions of simultaneous oxygen and glucose deprivation have been shown to trigger inflammasome assembly and pyroptotic IL-1β release (*8–11*), but the underlying mechanism has not yet been elucidated.

In recent years, the interplay between metabolism and immune function in myeloid cells has received intense attention. Three major metabolic changes in activated myeloid cells have been described (*12*). First, a rapid shift from oxidative phosphorylation towards glycolysis occurs, which ensures rapid supply with ATP and metabolites for energy intensive ribosomal biosynthesis and cytokine production (*13, 14*). Secondly, disturbances in the tricarboxylic acid cycle (TCA) result in the accumulation of succinate (*15*), which leads to stabilization of HIF-1a and *IL-1β* mRNA expression. Thirdly, increased flux through the pentose phosphate pathway (PPP) provides the NADPH required for maintaining a high cellular redox state and for synthesis of nucleotides, amino acids, fatty acid and membrane lipids (*2, 16*).

Glucose deprivation under hypoxia is likely to have a strong impact on all three of those distinctive metabolic features of activated myeloid cells. The goal of our study was, therefore, to investigate the consequences of the metabolic constraints present in vivo at sites of ischemia and chronic inflammation on activated myeloid cells, and to elucidate the mechanism behind inflammasome assembly and IL-1β release under glucose-oxygen deprivation.

RESULTS

Glucose deprivation under hypoxia induces inflammasome assembly and IL-1β release in monocytes

We have shown previously, that glucose deprivation alone has no influence on the function of activated monocytes and does not induce release of the myeloid master cytokine IL-1β (*17*). Concomitant hypoxia in combination with glucose deprivation, however, strongly induced release of IL-1β and IL-18 (Fig. 1A,B). Mature IL-1β and active caspase-1 could be detected in the supernatant after 5 and 7h, respectively (Fig. 1C). Enzymatic activity of caspase-1 was increased both in cell lysates and the supernatant of monocytes incubated under glucose deprivation and hypoxia at levels comparable to ATP stimulation (Fig.1 D,E). IL-1β release was dependent on ASC and caspase-1 (Fig. 1F,G) and accompanied by formation of ASC specks (Fig. 1H).

Glucose deprivation under hypoxia depleted the glycolytic pathway without significantly influencing TCA intermediates, while mitochondrial oxidative phosphorylation increased (Fig. S1A, S1B and S2A, S2B).

IL-1β release was accompanied by pyroptotic LDH release, which is caspase-1 dependent as shown with the caspase-1 deficient THP-1 cell line (Fig. 1I,J). Rescue experiments with re-introduction of glucose or oxygen into the cultures showed, that the induced metabolic changes and inflammasome activation are reversible (Fig. 1K). Surprisingly, experiments with monocytes from C57BL/6, BALB/c and DBA mice showed no IL-1β release (Fig. S3), which made experiments with genetically modified mice impossible.

Glucose deprivation under hypoxia depletes NADPH

Toll-like receptor (TLR)-triggered priming of monocytes is known not only to induce a rapid increase of glycolysis, but also to increase the fraction of metabolized glucose shunted through the PPP (*16*, *18*). Similarly, hypoxia has been shown to increase flux through the PPP in a range of cell types (*1*, *19*), thereby increasing efferocytosis (*20*).

Our metabolomic analysis of monocytes showed, that hypoxia increased concentrations of the first PPP metabolite, 6-phosphogluconate (6PG), likely as a result of increased PPP flux under this condition (Fig. 2A). Glucose deprivation under hypoxia led, as expected, to a marked reduction in levels of 6PG.

One major metabolic function of the PPP is the regeneration of NADPH concentrations to maintain the redox potential of the cell. Accordingly, NADPH measurements showed that glucose deprivation under hypoxia severely reduced monocyte NADPH concentrations (Fig. 2B). A corresponding trend towards increased concentration of $NADP^+$ did not reach statistical significance (Fig. 2C). The strained redox status of the cells was further illustrated by a significant decrease of NADH under glucose deprivation and hypoxia, although NAD^+ was unchanged (Fig. 2D,E).

The aforementioned reports on inflammasome activation under conditions of glucose deprivation and hypoxia investigated the role of reactive oxygen species (ROS), either of cytosolic (*8*) or mitochondrial origin (*9–11*), with conflicting results. To analyse mitochondrial ROS in our experimental setting, the fluorescence dye MitoSOX was used in flowcytometry, which showed no increase of mitochondrial ROS under glucose deprivation and hypoxia (Fig. 2F). The discrepancy with the published reports might in part be explained by the use of macrophages (*9–11*) or fibroblasts (*8*) and not monocytes in those experiments, and requires further investigation.

Based on the observed reduction of NADPH, we hypothesized that NADPH depletion due to inhibited PPP flux might contribute to the IL-1β release induced by glucose deprivation under hypoxia. Consistent with this hypothesis, inhibition of glucose-6-phosphate dehydrogenase (G6PD), the first step of the PPP, using 6-aminonicotinamide or dehydroepiandrosterone, induced high IL-1β release in monocytes incubated under hypoxia but did not further increase concentrations of IL-1β under glucose-oxygen deprivation (Fig. 2G,H). Activation of caspase-1 due to PPP inhibition with 6-aminonicotinamide under hypoxia was confirmed by Western blotting (Fig. 2I, S4). siRNA mediated knockdown of *G6PD* confirmed that specific inhibition of this enzyme, which leads to diminished flux through the PPP, triggers inflammasome activation and IL-1β release under hypoxia (Fig. 2J, K).

Impaired mevalonate kinase pathway leads to IL-1β release under glucose-oxygen deprivation

One major NADPH consuming pathway known to be associated with inflammasome activation is the mevalonate kinase pathway. Inhibition of its rate limiting enzyme, HMG-CoA reductase (HMGCR), has long been known to trigger inflammasome activation (*21–24*). In addition, the mevalonate kinase pathway is crucial in the induction of trained immunity in myeloid cells (*25*, *26*), which prompted us to investigate its role in IL-1β release of monocytes under glucose-oxygen deprivation.

HMGCR inhibition by simvastatin or atorvastatin triggered significant IL-1β release (Fig. 3A,B) and caspase-1 activation (Fig. 3C, S5) in the presence of glucose and/or oxygen, which indicates that full flux through the mevalonate kinase pathway is required to prevent inflammasome activation and IL-1β release. Importantly, HMGCR inhibition had no additional

stimulatory effect on IL-1β release under glucose-oxygen deprivation, indicating that the pathway is already inhibited by glucose deprivation under hypoxia (Fig. 3A,B).

AMPK activation under hypoxia contributes to inhibition of mevalonate kinase pathway

The cellular energy sensor AMPK, which has been shown to be activated not only by energy deficiency, but also by hypoxia in many cell types and by various pathways (*27–30*), was found to be activated under glucose deprivation and hypoxia (Fig. 3D). Experiments with the AMPK inhibitor dorsomorphin showed, that active AMPK is required for IL-1β release induced by glucose-oxygen deprivation (Fig. 3E).

HMGCR activity is regulated in part by AMPK which phosphorylates and thereby inhibits it (*31*). Accordingly, the AMPK activator AICAR was found to induce IL-1β release in the presence of glucose and/or oxygen (Fig. 3F). Of note, AICAR had no additional stimulatory effect on monocytes under glucose-oxygen deprivation, again indicating that HMGCR is already inhibited due to AMPK activation under those conditions.

Monocytes are characterized by high HMGCR activity due to high mRNA expression levels of SREBP-2 target genes involved in the mevalonate kinase pathway (*32*), and this includes high mRNA expression of *HMGCR*. Quantification of *HMGCR* mRNA showed it to be downregulated under glucose deprivation and hypoxia (Fig. 3G), possibly as a result of SREBP-2 inhibition due to AMPK activation.

HMGCR is also regulated by endoplasmic reticulum-associated degradation, which in turn is known to be increased by hypoxia (*33–35*). Determination of HMGCR protein content showed that concentrations of the enzyme were also significantly reduced under glucose-oxygen deprivation (Fig. 3H).

Protein hypoprenylation triggers IL-1β release of monocytes

Inhibition of the mevalonate kinase pathway leads to reduced synthesis of the isoprenoids farnesylpyrophosphate (FPP) and geranylgeranylpyrophosphate (GGPP). FPP and GGPP are the substrates required for protein prenylation. GGPP deficiency has been found to trigger inflammasome activation (*21*, *22*, *36*) and inflammatory tissue injury (*37*).

We quantified FPP and GGPP and found a significant reduction under glucose deprivation and hypoxia compared to control conditions (Fig. 4A,B). Both FPP and GGPP supplementation were able to significantly inhibit the IL-1β release induced by glucose deprivation under hypoxia (Fig. 4C). Since the synthesis of GGPP from FPP is not reversible, this confirms, that lack of prenylation substrates and not deficient cholesterol and sterol synthesis triggers the IL-1β release induced by glucose-oxygen deprivation. Accordingly, squalene supplementation had no effect on IL-1β release (Fig. 4D), while geranylgeranyltransferase type I (GGTase-I) inhibition was found to induce IL-1β release in the presence of glucose and/or oxygen, but had no effect under glucose deprivation and hypoxia (Fig. 4E).

To further corroborate the link between mevalonate kinase pathway, GGPP deficiency restricting protein prenylation, and caspase-1 activation, we substituted FPP or GGPP in cultures with atorvastatin. The results show that statin-induced IL-1β release is abrogated by isoprenoid supplementation, while nigericin-induced inflammasome activation is not (Fig. 4F).

Monocytes from mevalonate kinase deficient patients are hyperactivated by hypoxia

Shortage of GGPP and FPP leading to defective protein prenylation is known to be the underlying cause of monocyte hyperactivation in the genetic disorder mevalonate kinase deficiency (MKD) syndrome. We analyzed monocytes from pediatric patients with homozygous MKD and compared them to their heterozygous, healthy mothers.

Incubation of MKD monocytes under hypoxic conditions in the presence of glucose was found to induce significantly higher IL-1β concentrations compared to the controls (Fig. 5A). This indicates that in individuals with a genetically compromised mevalonate kinase pathway, hypoxia triggers a similar inflammatory response as glucose-oxygen deprivation does in healthy controls.

GGPP deficiency under glucose-oxygen deprivation activates not the pyrin, but the NLRP3 inflammasome

Recently published studies have linked MKD to activation of the pyrin inflammasome. Hypoprenylation of two small GTPases, RhoA (*38*) and Kras (*39*), was shown to trigger assembly of the pyrin inflammasome, caspase-1 activation, and IL-1β release. To determine the role of pyrin in IL-1β release under glucose deprivation and hypoxia, we performed Crispr/Cas9 mediated deletion of *MEFV* in THP-1 cells and siRNA knockdown of *MEFV* in monocytes. Genetic inhibition of *MEFV* did not reduce IL-1β levels which ruled out a significant role for the pyrin inflammasome under glucose-oxygen deprivation (Fig. 5B,C). Confirmation of the Crispr/Cas9 mediated gene deletion was obtained by next-generation sequencing (Fig. S6), and siRNA mediated knockdown was verified by Western blotting (Fig. S7).

More recent reports have shown, that lack of protein prenylation in MKD patients or in patients treated with statins also triggers activation of the NLRP3 inflammasome (*36*, *37*, *40–42*). siRNA mediated knockdown of *NLRP3* in monocytes (Fig. 5C) and experiments with NLRP3 deficient THP-1 cells (Fig. 5D) showed, that NLRP3 is essential for IL-1β release under glucose deprivation and hypoxia. Accordingly, the supernatant of monocytes incubated under those conditions contained higher protein amount of NLRP3 compared to controls (Fig. 5E). Immunoprecipitation experiments confirmed unequivocally that the NLRP3 inflammasome was assembled under glucose deprivation and hypoxia, since they showed NLRP3 bound to ASC in monocyte lysates (Fig. 5F and fig. S8).

Finally, we investigated IL-1β release of monocytes from patients with an activating mutation in NLRP3 (Muckle-Wells syndrome, MWS). As expected in this disease, the LPS response in the presence of glucose and oxygen was pathologically increased. Glucose deprivation under hypoxia triggered an even higher IL-1β release that significantly exceeded that of healthy controls, implicating the mutated NLRP3 inflammasome in this process (Fig. 5G).

Non-prenylated Rac1 links GGPP depletion to NLRP3 inflammasome activation

Besides RhoA and Kras, the small GTPase Rac1 has also been implicated in the autoinflammatory diseases MKD and Familial Mediterranean Fever (FMF) (*43*, *44*) and was shown to activate NLRP3 in kidney disease (*45*, *46*). In a GGTase-I knockout mouse model, non-prenylated Rac1 mediates NLRP3 activation and excessive IL-1β release (*47*, *48*). Therefore, we investigated the role of Rac1 in IL-1β release under glucose-oxygen deprivation using the specific Rac1 inhibitor NSC23766.

Inhibition of Rac1 abrogated IL-1β release and inhibited caspase-1 activation in monocytes cultured under glucose-oxygen deprivation but had no effect under standard culture conditions (Fig. 6A,B and Fig. S9). A second pharmacologic inhibitor of Rac1, EHT1846, had a less marked but similar effect, thereby confirming the pivotal role of Rac1 in this process (Fig. 6C).

Quantification of non-prenylated and prenylated Rac1 in lysates of monocytes by Western blot confirmed, that glucose deprivation under hypoxia leads to an increase of non-prenylated Rac1 (Fig. 6D).

The PPP inhibitor 6-aminonicotinamide was used to confirm the link between PPP-dependent NADPH regeneration and Rac1 prenylation. As expected, PPP inhibition increased the ratio of non-prenylated to prenylated Rac1 in a manner similar to that seen under glucose deprivation and hypoxia (Fig. 6E).

Experiments with peripheral blood monocytes from two adult patients with mevalonate kinase deficiency also indicated an increased fraction of non-prenylated Rac1 already under hypoxic conditions in the presence of glucose in those patients (Fig. S10).

Recently, non-prenylated Rac1 has been found to bind the adaptor protein Ras GTPase-activating-like protein 1 (IQGAP1) with threefold increased affinity (*48*), and this binding mediates inflammasome assembly. Knockdown of *IQGAP1* by siRNA under glucose-oxygen deprivation also led to a significant reduction in IL-1β release (Fig. 6F,G). Accordingly, we propose that non-prenylated Rac1 under glucose-oxygen deprivation triggers NLRP3 inflammasome activation by increased binding to IQGAP1 (graphical illustration of the pathway Fig. 6H).

DISCUSSION

We report here that inflammasome activation in monocytes maintained under both glucose deprivation and hypoxia results from protein hypoprenylation, which in turn is a consequence of a reduction in NADPH levels leading to restriction of the mevalonate kinase pathway and isoprene deficiency.

The increased PPP flux in myeloid cells exposed to hypoxia has recently been described in detail (*20*). We report here that the combined effect of glucose deprivation and hypoxia suppresses the PPP and reduces cellular NADPH concentration. As well as having important implications for the redox status of the cell, this also leads to a suppression of the mevalonate kinase pathway, since NADPH is an essential cofactor of HMGCR. Pharmacological inhibition of HMGCR has long been known to induce inflammasome activation and IL-1β release (*8–11*). We show here that restoration of the mevalonate pathway *in vitro* is sufficient to reduce inflammasome activation under glucose deprivation and hypoxia, suggesting that a pharmacological increase in flux towards the isoprenoid lipid molecule GGPP may be a feasible anti-inflammatory therapeutic approach for chronic inflammatory conditions. However, it should be noted that over-stimulation of the mevalonate pathway has been shown to contribute to fibrosis mediated through Rac1 activation (*49*).

Isoprene deficiency limits prenylation of newly synthesized proteins in the endoplasmic reticulum. Under glucose deprivation and hypoxia, it is the hypoprenylation of Rac1 that triggers NLRP3 inflammasome activation and IL-1β release. The triggering of NLRP3 inflammasome assembly by non-prenylated Rac1 has already been shown to occur in cases of human genetic mevalonate kinase deficiency (MKD) (*36*, *37*, *40–42*). However, while the isoprene deficiency in MKD also leads to hypoprenylation of proteins such as RhoA (*39*) or Kras (*38*) and subsequent activation of the pyrin inflammasome, we have excluded a role for the pyrin inflammasome in monocytes under glucose deprivation and hypoxia. The relatively mild phenotype seen as a consequence of glucose deprivation and hypoxia *in vitro* differs markedly from that of MKD, in which hyperactivation of macrophages is already apparent under normoxic conditions. Indeed, the clinical course of MKD is often very severe and is likely to result from compromised sterol synthesis and from the accumulation of mevalonic acid in addition to GGPP deficiency.

In the mouse model with a GGTase-I deletion in myeloid cells, hypoprenylation of Rac1 triggers an erosive polyarthritis resembling rheumatoid arthritis (RA) (*47*), which can be alleviated by inactivating IQGAP1 (*48*). Interestingly, IQGAP1 has recently been reported to be genetically linked to RA in humans (*50*). The involvement of the mevalonate kinase pathway in RA is evidenced by the increased risk of RA (*51*) and accelerated onset of collagen type II-induced arthritis (*52*) in mice treated with statins to inhibit HMGCR activity.

Along the same lines, earlier reports of the clinical efficacy of Rac1 inhibition in animal models are of particular interest, although they were performed before a pathogenetic link between Rac1 and arthritis had been discovered. These results showed that blockade of Rac1 activation either by a pharmacological inhibitor or by an inhibitory peptide can lead to clinical improvement of murine arthritis (*53*, *54*). Similarly, in vitro depletion or pharmacological inhibition of Rac1 has also been shown to reverse destructive and aggressive tumor-like properties of fibroblast-like synoviocytes from rheumatoid arthritis patients, indicating that inhibition of Rac1 in non-myeloid cells might also be clinically beneficial in RA (*55*). Intriguingly, Rac1 has also been shown to be inhibited by thiopurines such as azathioprine, both in T cells (*56*) and endothelial cells (*54*), due to specific blockade of Rac1 following binding to azathioprine-generated 6-thioguanine triphosphate (6-Thio-GTP) instead of GTP. Although not widely used, azathioprin also improves joint inflammation in RA (*57*), underlining the potential of the Rac1 pathway as a therapeutic target in RA.

The apparent discrepancy between the responses of human and mouse monocytes to glucose deprivation and hypoxia requires further investigation. One possible explanation for this difference might involve species-specific differences in the metabolism of acetyl-CoA. The breakdown of citrate by ATP-citrate lyase is a primary source of cytoplasmic acetyl-CoA (*58*). The enzyme ATP-citrate lyase is up to fourfold more active in mice (*59*), and any increase in abundance of acetyl-CoA supplying the mevalonate kinase pathway might explain the greater resistance of mouse monocytes against glucose deprivation and hypoxia. A further discrepancy between human and mice innate immune responses is found in the *pyrin* gene. Mouse pyrin is known to lack the C-terminal domain, termed B30.2, that is present in the human protein, and major differences in the regulation of the gene have been noted between human and mouse (*60*). Although our results indicate that pyrin is not the primary inflammasome sensor responsive to oxygen and glucose deprivation, it might still play a regulatory role in NLRP3 activation as has been previously suggested (*61*).

In conclusion, we have found that concomitant oxygen and glucose deprivation suppresses mevalonate synthesis and protein prenylation in macrophages, resulting in Rac1 hypoprenylation and IQGAP1-mediated inflammasome activation. Interference with mevalonate synthesis or protein prenylation were found to induce IL-1β release even in the presence of oxygen and glucose. In contrast, pentose phosphate pathway inhibition triggered inflammasome activation only under hypoxia, which is likely due to an inhibitory effect of hypoxia on HMGCR abundance and activity.

To the best of our knowledge, this is the first report linking regulation of the mevalonate kinase pathway to pathological inflammation in acquired diseases rather than inherited autoinflammatory syndromes.

MATERIALS AND METHODS

Experimental model and subject details

Human study and approval

For the experiments with human monocytes, healthy blood donors were recruited in accordance with the Declaration of Helsinki under a protocol approved by the Ethics Committee of the Medical Faculty of the University of Leipzig (313/14-ek and 430/16-ek). Studies with patients with Muckle-Wells syndrome (MWS) and mevalonate kinase deficiency (MKD) were conducted in accordance with protocols approved by the Ethics Committee of the Medical Faculty of the University of Leipzig (050/20-ek) and the Ethics Review Board of the Charité – Universitätsmedizin Berlin (EA2/154/15), respectively. All blood donors or their legal representatives gave written informed consent. The patients with Muckle-Wells syndrome associated with the NALP3 variant R260W (MWS, 1 female and 1 male, with average age of 83 years) were part of a family reported previously (Haas et al., 2004). Age-and sex-matched healthy control subjects were recruited among the healthy blood donors. In addition, 5 patients with mevalonate kinase deficiency (MKD) were enrolled, including 2 male adults with an average age of 24 years and 3 patients (1 female and 2 male) with an average age of 4 years. Their mothers served as healthy controls.

Mice study and approval

DBA/2 Mice were purchased from Janvier Labs. C57BL/6J and SKG mice were bred and maintained under SPF conditions in the Medizinisch Experimentelles Zentrum (MEZ) Medical Faculty of the University Leipzig. Healthy, adult (> 8 weeks) male and female mice were sacrificed with the approval of the local regulatory agency.

Cell lines and primary cell culture

Primary human monocytes and all cell lines were cultured at 37 °C in a 5 % CO_2 humid atmosphere. Isolated monocytes were cultured in RPMI medium supplemented with 1 X GlutaMax, 10 % FBS and 5 mM glucose or without glucose (0 mM). MEFV knockout THP-1 cells were grown in RPMI 1640 containing 10 % FBS. The selection antibiotics blasticidin (10 µg/ml) and puromycin (0.8 µg/ml) were added once a week. THP-1 cells deficient for ASC, caspase-1, NLRP3 (def ASC, def CASP1, def NLRP3) and the control cells (def Null) and the THP-1 DSMZ cells were grown in RPMI 1640 containing 10 % FBS and 1 % penicillin and streptomycin (pen/strep). The selection antibiotic hygromycin B gold (200 µg/ml) was added to the deficient cell lines at each passage. For cell culture of THP-1-ASC-GFP cells the selection

antibiotic zeocin (100 µg/ml) was added. Normoxic cell culture was performed under atmospheric oxygen (21%). For hypoxic cell culture conditions, cell culture plates were sealed in a hypoxia bag filled with a gas mixture consisting of 1 % O_2, 5 % CO_2 and 94 % N_2. Hypoxia stimulation samples were treated continuously at 1 % O_2 in a hypoxia box. The different treatment conditions for the various in vitro assays are listed in the method details section.

Method details

Monocyte Isolation

Human peripheral blood mononuclear cells (PBMCs) were isolated from healthy donors, patients with MKD or MWS by Ficoll-Paque density gradient centrifugation. After several washes with 1 X PBS/0.3 mM EDTA monocytes were obtained by negative separation using the monocyte isolation kit II according to the manufacturer's protocol.

CRISPR/Cas9 knockout of MEFV in THP-1 cells

Transduction of THP-1 cells was performed with lentiviral Cas9 particles (Dharmacon, Edit-R Lentiviral hEF1α-Blast-Cas9 Nuclease Particles, cat. VCAS10126). 5 x 10^5 cells per 250 µl RPMI 1640 containing 1 % FBS without antibiotics were transduced with MOI 3. 16h after transduction a medium change was performed (500 µl RPMI 1640/10 % FBS). After another 48h, the selection antibiotic blasticidin (10 µg/ml) was added to the cell culture medium and the selection was carried out for one week. An antibiotic kill curve was prepared in advance to determine the concentration of the selection antibiotics blasticidin and puromycin.

Western blot was performed to verify the Cas9 protein expression. Subsequently, Cas9-transduced THP-1 cells were transduced a second time with lentiviral particles containing sgRNAs against MEFV (Dharmacon, Edit-R Lentiviral mCMV-Puro sgRNA particles, clone VSGHSM_26692266, DNA target sequence 5′- AGCAGAGTGGCCATCTTCAC-3′, cat. no. VSGH10142-246536801) or a non-targeting control sequence (Edit-R Lentiviral mCMV-Puro non-targeting sgRNA particles, cat. VSGC10216). After 48h, the antibiotic puromycin (0.8 µg/ml) was added to the cell culture medium to select the transduced cells. Further cell culture was conducted as described in experimental model and subjects section.

A p24 ELISA was performed to ensure that the transduced cells did not secrete virus particles. Assay was done according to manufacturer's instructions. Cells were seeded as single cell clones into wells of a 96-well U-bottom plate on the BD FACS Aria III cell sorter (Core Unit Fluorescence Technology, Leipzig University). To support cell growth-conditions, conditioned

medium from a running THP-1 cell culture was mixed 1:1 with RPMI 1640 supplemented with 10 % FBS and 1 % pen/strep, but without selection antibiotics. After 3 weeks of cell growth, clones were subjected to a mismatch detection assay. The primer sequences for mismatch detection in the MEFV gene were designed to encompass the sgRNA target site (forward 5′-GAAAGGGACGTTCCTGAACTA-3′ and reverse 5′- GTAAGAAGAGAACACAGCCG-3′). For further assays, one clone with a mismatch in the MEFV site (MEFV 66) and a control clone without a mismatch (Ctrl216 B6) were used. To confirm successful knockout, the MEFV gene in clones was analyzed by deep sequencing as published previously (Jäger et al. 2020). Nextera DNA library preparation (Illumina) and sequencing of PCR products in the DNA Core Unit (University of Leipzig) confirmed the deletion of 25 base pairs in the target sequence. All MEFV 66 sequences contained deletion which effectively excluded the persistent presence of the wild-type gene. No deletion was present in the Ctrl216-B6 cells.

Mice

Male and female C57BL/6J, BALB/c and DBA/2 mice were bred and maintained under SPF conditions in the Medizinisch Experimentelles Zentrum (MEZ) Medical Faculty of the University Leipzig. Adult mice (> 8 weeks) were sacrificed and peripheral blood was sampled with a heparinized syringe through heart puncture. PBMCs were obtained following Ficoll-Paque density gradient centrifugation of the pooled blood samples. Isolation of CD11b-positive monocytes was achieved with the CD11b MicroBeads kit, following the instruction manual. Monocytes were seeded at a density of 1 $x10^6$ cell per 200 µl in a 96-well plate in RPMI (1 X GlutaMax, 10% FBS, 5 mM or 0 mM glucose), primed with 100 ng/ml LPS and cultured under normoxic or hypoxic conditions. As a positive control for inflammasome activation cells were treated with 2.5 mM $CaCl_2$.

In vitro stimulation assays

Primary human monocytes were seeded at a concentration of 3 $x10^5$ per 200 µl cell culture medium supplemented with 5 mM glucose or without glucose (0 mM) in 96-well plates. Monocytes were cultured under either normoxic or hypoxic conditions for the indicated time points in presence of 100 ng/ml LPS. For in vitro stimulation experiments with THP-1 cells (MEFV knockout, THP-1 def Null/def ASC/def Casp1/def NLRP3, THP-1 DSMZ or THP-1-ASC-GFP), 5 $x10^5$ cells were differentiated in 1 ml cell culture medium containing 50 ng/ml phorbol-12-myristate-13-acetate (PMA) for 2 days in 24-well plates. Afterwards, cells were primed with 100 ng/ml LPS in RPMI supplemented with 1 X GlutaMax, 10 % FBS and 5 mM

glucose or without glucose (0 mM) under normoxic or hypoxic conditions for indicated time points. For the various cell culture experiments, the following activators, inhibitors and reagents at the indicated concentrations were co-incubated throughout the stimulation period.: 5-aminoimidazole-4-carboxamide-1-β-D-ribofuranosyl 5′-monophosphate (AICAR), adenosine triphosphate (ATP), atorvastatin (AS), dehydroepiandrosterone (DHEA), dorsomorphin (Dorso), EHT 1864, geranylgeranyltransferase type I inhibitor 298 (GGTI 298), monosodium urate crystals (MSU), NSC 23766, simvastatin (Simva), 6-aminonicotinamide (6-AN), squalene (SQ), farnesyl pyrophosphate (FPP) and geranylgeranyl pyrophosphate (GGPP). For the supplementation of FPP and GGPP an appropriate solvent control specified by the manufacturer (methanol: 10mM NH_4OH (7:3)) was included.

Rescue assay

3 x10^5 monocytes per 200 µl cell culture medium without glucose (0 mM) were primed with LPS (100 ng/ml) in a 96-well plate under hypoxic conditions. After 1 h, 4 h, 6 h, or 8 h, either glucose (5 mM) was added to the cell culture medium under hypoxic conditions or the plate was re-oxygenated. The incubation time of each approach was 16 h in total.

Lactate-Dehydrogenase Cytotoxicity Assay

The Pierce Lactate-Dehydrogenase (LDH) Cytotoxicity Assay Kit was used to determine cellular vitality. THP-1 cells were seeded in duplicates at a concentration of 5 ×10^5 cells per 1 ml cell culture medium in 24-well plates. Following differentiation with 50 ng/ml PMA for 2 days, LPS-primed (100 ng/ml) cells were incubated in RPMI supplemented with 1 X GlutaMax, 10 % FBS and without glucose (0 mM) under hypoxic conditions for the indicated time points. Lactate dehydrogenase was determined in lysed cells (after addition of 20 µl 9% Triton X-100 solution) and in the supernatant according to the assay instructions. Cytotoxicity was calculated using the following equation:

$$\%\ cytotoxicity = \frac{\text{LDH activity supernatant} * 100\%}{\text{LDH activity supernatant of lysed cells}}$$

Detection of human and mouse IL-1β and IL-18

Human IL-1β and IL-18 were determined in the cell culture supernatants of LPS-primed monocytes and THP-1 cells using the IL-1β ELISA Set II and the IL-18 ELISA, respectively. For detection of secreted mouse IL-1 β, the mouse IL-1 β uncoated ELISA kit was used. ELISA were performed according to the manufacturer`s instructions.

Caspase-1 activity assay

Caspase-1 activity was determined in cell culture supernatant and directly in monocyte cell culture using the Caspase-Glo 1 Inflammasome Assay according to the manufacturer's protocol. Briefly, for determination in cell culture supernatant, 50 µL of cell culture supernatant (1.5 $x10^6$/ml) was transferred to a white 96-well plate, mixed 1:1 with Glo1 reagent, and incubated as a duplicate for one hour at room temperature. For cell culture activity determination, half of the cell culture supernatant was discarded from the incubated monocytes (3 $x10^5$/200µl) and the volume was replaced with Glo1 reagent for one hour incubation. The luciferase signal of the samples and the corresponding controls was measured using a SPARK multimode microplate reader (Tecan GmbH). In parallel, nonspecific protease activity was determined using Ac-YVAD-CHO (caspase-1 inhibitor)-containing Glo1 reagent and subtracted from the respective measured values as background.

siRNA mediated knockdown of *MEFV, NLRP3, IQGAP1*, and *G6PD*

6 $x10^5$ monocytes per 400µl RPMI 1640 supplemented with 10 % FBS, 5 mM glucose and 100 ng/ml IFN-γ were seeded in 48-well plates and transfected with 50 nM siRNA mix. For the siRNA mix, Viromer Green was mixed with Viromer Buffer Green according to the Lipocalyx company's instructions. 1 µM of control siRNA-E, MEFV- or NLRP3-siRNA were complexed with the Viromer Green solution and incubated for 15 min at room temperature (RT). After 16 h of incubation the transfected monocytes were washed with 1 X PBS and lysed for Western blot analysis or primed with 100 ng/ml LPS in RPMI supplemented with 1 X GlutaMax, 10 % FBS and 5 mM glucose or without glucose (0 mM) under either normoxic or hypoxic conditions for 8 h.

For siRNA-mediated knockdown of *IQGAP1*, 1 $x10^5$/ml THP-1 DSMZ cells were seeded overnight. Afterwards, cell number was determined and 5 $x10^5$ cells per 1 ml cell culture medium were transfected with 100 nM siRNA mix of control siRNA-E or IQGAP1-siRNA for 5 h. Subsequently, cells were washed with 1 X PBS and differentiated with 50 ng/ml PMA for 2 days. After that, cells were either lysed for Western blot analysis or primed with 100 ng/ml LPS in RPMI supplemented with 1 X GlutaMax, 10 % FBS and 5 mM glucose or without glucose (0 mM) under either normoxic or hypoxic conditions for 8h.

For siRNA-mediated knockdown of *G6PD* the tyrosine-modified low-molecular weight polyethylenimine (LP10Y) polymer was used (*62*). For this, 1 $x10^6$ monocytes per 500 µl RPMI 1640 supplemented with 10% FBS, 5 mM glucose and 100 ng/ml IFN-γ were seeded in a 24-

well plate and transfected with 45 pmol siRNA. For the siRNA/polymer mix, G6PD siRNA or control siRNA-E was complexed with LP10Y polymer (ratio: 1 µg siRNA: 2.5 µg LP10Y polymer) in trehalose buffer and incubated for 30 min at room temperature (RT). After 16 h incubation, the transfected monocytes were washed with 1 X PBS and primed with 100 ng/ml LPS in RPMI supplemented with 1 X GlutaMax, 10 % FBS and 5 mM glucose or without glucose (0 mM) under either normoxic or hypoxic conditions for 8 h.

Fluorescence microscopy of ASC speck formation in THP1-ASC-GFP cells

THP1-ASC-GFP cells expressing ASC-GFP fusion protein (Invivogen), were differentiated with 100 ng/ml PMA in RPMI 1640 with 11mM Glucose and 10% FBS. After 24h, the medium above the adherent cells was removed and replenished with fresh RMPI (1 X GlutaMax, 10 % FBS) with 5 mM glucose or without glucose (0 mM). Following LPS priming (100 ng/ml), cells were incubated for 16h under normoxic or hypoxic conditions. GFP-fluorescence of cytosolic ASC or in ASC-specks was visualized after laser excitation with a fluorescence microscope (Olympus IX50) and the software cellSens Entry.

Cell lysis, gel electrophoresis and Western blot analysis

In a 24-well plate, 1.5 x10^6 monocytes per 1 ml cell culture medium supplemented with 5 mM glucose or without glucose (0 mM) were primed with 100 ng/ml LPS and incubated under normoxic or hypoxic conditions for the indicated periods. After incubation, cell culture supernatants were removed and adherent cells were washed once with 1 X PBS before lysis. For protein analysis of caspase-1, IL-1β, IQGAP1, NLRP3, pAMPKα T172, Vinculin and β-Actin by Tris-Glycine SDS-PAGE (10 %, 12 % or 15 % depending on the molecular weight of the protein of interest), cells were lysed on ice for 15 min with buffer containing 70 mM Tris (pH 7.8), 137.5 mM NaCl, 2 mM EDTA, 10 % glycerol, 1 % IGEPAL CA-630, complete protease inhibitors and PhosStop. To detect the proteins caspase-1, IL-1β, NLRP3, pAMPKα T172 and β-Actin lysed cells were centrifuged (10000 g, 15 min, 4 °C) and the protein content was determined in the supernatant by Detergent Compatibility Assay from BioRad (DC-Assay) according to manufacturer's protocol. For detection of IQGAP1 and vinculin lysed cells were sonicated (30 sec/ 2/2/ 70 % amplitude) and the whole cell lysate was used for DC-Assay. Whole cell lysate were mixed with reducing Laemmli and samples were boiled for 5 min at 95 °C before equal amounts of protein were subjected to SDS-PAGE. For analyzing time-dependent release of IL-1β and caspase-1 500 µl supernatant was centrifuged through a 50k-Amicon ultra column (Merck Millipore) (14.000g,10min, 4°C) to remove all proteins larger

than 50 kDa. Afterwards the flow-through was concentrated with a 3k-Amicon-ultra column (Merck Millipore) (14.000g, 30min, 4°C), mixed with reducing Laemmli and boiled.

For the detection of caspase-1 activation (p20 Subunit) of 16h stimulated monocytes (3 x10^5 monocytes/120 µl; treated with 50 µM 6-AN, 10 µM Atorvastatin, 10 µM NSC23766) aliquots (37.5 µl) of the supernatants were supplemented with Laemmli buffer, boiled and subjected to SDS-PAGE. Equal loading gel blotting onto the membrane was shown with Ponceau S staining for 10min.

For detection of non-prenylated and prenylated Rac1 by Western blot, cells were lysed on ice for 30 min with a lysis buffer containing 50 mM Hepes, 150 mM NaCl, 1% NP-40, 0.25 % sodium deoxycholate, 1 mM EDTA, 1 mM PMSF, 1 mM NaF, 1 mM Na_3VO_4, and complete protease inhibitors, followed by a 10 min centrifugation step at 13000 rpm at 4°C. The supernatant was used for the DC assay. Aliquots containing equal amounts of protein were mixed with non-reducing loading buffer (NuPAGE) and boiled for 5 min at 95 °C before samples were resolved by SDS-PAGE using 12 % Tris-Bis gel (NuPAGE, cat. no. NP0341) according to manufacturer's instruction.

Using the wet electroblotting system according to the manufacturer`s protocol, the resolved samples were transferred to a polyvinylidene difluoride (PVDF) membrane. The PVDF-membrane was blocked with 5 % skim milk in TBS-T (10 mM Tris (pH 8.0), 150 mM NaCl, 0.5 % TWEEN 20) for 60 min, then washed three times for 5 min in TBS-T and incubated with primary antibody against ASC, Caspase-1, GAPDH, IL-1β, NLRP3, IQGAP1, pAMPKα T172, Rac1, Vinculin or β-Actin overnight at 4°C. After three washes with TBS-T, 5 min each, membrane was incubated with the appropriate HRP-conjugated secondary antibody, anti-mouse IgG-HRP or anti-rabbit IgG-HRP (dilution 1 : 10000 in TBS-T) for 60 min at RT. Membrane was developed using ECL system. Quantification of the determined band intensities was performed using ImageJ software.

Immunoprecipitation (IP) of NLRP3

5 x10^5 THP-1 DSMZ cells were differentiated in 1 ml cell culture medium (100 ng/ml PMA) for 2 days before being primed with 100 ng/ml LPS (1 X GlutaMax, 10 % FBS, 0 mM glucose) at the indicated time points under hypoxic conditions. Cells were washed once with 1 X PBS and lysed by adding Kehrl-buffer (200 mM Hepes, 50 mM glycerol 2-phosphate, 1 mM Na_3VO_4, 0.50 % Triton X-100, 0.50 % CHAPS, 10 % glycerol, complete protease inhibitors). 10 % of the cell lysate was used as input and 0.5 mg-1 mg for immunoprecipitation with the protein G magnetic beads. These were previously coupled (1 h, 4 °C) to the Cryopyrin antibody

(4 µg, cat. no. sc-66846) or IgG isotype control (cat. no. sc-2027). After washing with Kehrl-buffer, bead-antibody-mix was added to cell lysate and incubated over night at 4 °C. Subsequently, the lysate-bead-antibody mixture was washed three times with high-salt wash buffer (20 mM Hepes, 2 mM EDTA, 1 M NaCl, 0.1 % SDS, 1 % Triton X-100) or with 1 X PBS/0.02 % TWEEN. After elution (0.1 M glycine (pH 2.5)), samples were mixed with 1 X reducing Laemmli, boiled (5 min, 95 °C), and subjected to SDS-PAGE and Western blot.

Quantitative detection of HMGCR by ELISA

In a 24-well plate coated with 1.5 % agarose, 1.8 x10^6 monocytes were primed with LPS (100 ng/ml) in 1.2 ml cell culture medium with 5 mM glucose or without glucose (0 mM) under normoxic or hypoxic conditions for 6 h. After stimulation, the cell suspension was centrifuged at 10000 g for 2 min at 4 °C, the supernatant removed and the cell pellet resuspended in 250 µl cold 1 X PBS (1000 g, 5 min, 4 °C) after washing twice with precooled 1 X PBS. Subsequently, cells were disrupted by sonication (8 sec, 2/2, 30 % amplitude) and centrifuged again (1500 g, 15 min, 4 °C). The supernatant obtained was used for the human 3-hydroxy-3-methylglutaryl coenzyme A reductase (HMGCR) ELISA kit from MyBioSource for the quantification of the protein content. The ELISA was performed according to the manufacturer's instructions.

NAD+/NADH and NADP+/NADPH protein measurement

Intracellular NAD+/NADH and NADP+/NADPH was quantified with the PicoProbe Quantitation Fluorometric kit. In brief, isolated monocytes were seeded at a density of 3 x 10^5 cells per 200 µl RPMI 1640 (1 X GlutaMax, 10 % FBS, with 0 mM or 5 mM glucose) in a 96-well plate. Cells were treated for the indicated times with LPS (100 ng/ml) under normoxic or hypoxic conditions. Afterwards the supernatant was discarded and the cells lysed in 150 µl extraction buffer. The NAD+/NADH and NADP+/NADPH concentration was analyzed following the instruction manual. Total protein content of the lysates was determined with the DC Assay.

Measurement of mitochondrial ROS with MitoSOX

Monocytes (6x10^5 / 500 µl) were cultured under normoxic or hypoxic conditions in RPMI 1640 (1 X GlutaMax, 10 % FBS, with 0 mM or 5 mM glucose) treated with LPS (100 ng/ml) for 6h. After removing the supernatant, the cells were treated with 500 µl of 5µm MitoSOX solution for 15min at 37°C under normoxic or hypoxic conditions. Then cells were washed and MitoSOX fluorescence was analyzed via flow cytometry. Hypoxic probes were treated the

whole time under hypoxic conditions. Rotenone (10 µM) was used as positive control and subjected to the cells prior to the measurement.

Measurement of intracellular polar metabolites using Ion Chromatography Mass Spectrometry (IC-MS)

The intracellular concentration of the metabolites were determined in 1 $x10^6$ monocytes cultured in 700 µl cell culture medium supplemented with 5 mM glucose or without glucose in agarose-coated 24-well plates. After LPS-stimulation (100 ng/ml) for the indicated time points under normoxic or hypoxic conditions, cells were harvested and washed once with 1 X PBS. The pellet was dissolved in in 500 µl 45 % (v/v) methanol/5 % (v/v) chloroform. After the addition of 500 µl water the suspension was mixed 30 min at 4 °C. The solution was centrifuged at 500 g for 10 min, the upper phase was transferred and vacuum dried. For determination of polar metabolites using ion chromatography coupled to tandem mass spectrometry (IC-MS/MS) cell pellets were extracted as described above and supernatants were ten-fold diluted in Milli-Q water and analyzed on an ICS-5000 (Thermo Fisher Scientific) coupled to an API 5500 QTrap-MS (AB Sciex, Concord, Canada) as described previously (*63*). Separation was achieved on IonPac AS11-HC column (2 x 250mm, Thermo Fisher Scientific) with increasing potassium hydroxide gradient. The initial composition of the eluent was 1 mM KOH held for 7 min, followed by a linear gradient to 5 mM within 10 min, held for another 4 min. Thereafter, the KOH concentration was changed to 25 mM within 8 min and afterwards to 100 mM within 32 min. The final concentration was held for another 8 min with a subsequent 10 min re-equilibration step to the initial composition of the system. MS analysis was performed in multiple reaction monitoring (MRM) mode using negative electrospray ionization and included organic acids, carbohydrates and nucleotides involved in central metabolite pathways e.g. glycolysis, TCA-cycle, energy metabolism as well as pyruvate Metabolites were considered to be detectable above a signal-to-noise ratio (S/N) of three within a retention time window of 0.5 min. Optimized MS-parameters were as following: ionspray voltage −4500 V, nebulizer gas (GS1), auxiliary gas (GS2), curtain gas (CUR) and collision gas (CAD) were 30, 50, 20, medium (arbitrary units), respectively. The source temperature was maintained at 450 °C. Declustering potential (DP), collision energy (CE), entrance potential (EP) and collision cell exit potential (CXP) were optimized separately for each analyte by infusion.

Measurement of Farnesyl pyrophosphate (FPP) and Geranylgeranyl pyrophosphate (GGPP) using High Performance Liquid Chromatography (HPLC)

In a 24-well plate coated with 1.5 % agarose, monocytes ($1x10^6$/700µl) were primed for 6 h with LPS (100 ng/ml) in cell culture medium supplemented with 5 mM glucose or without glucose under normoxic or hypoxic conditions. Cells were harvested, washed once with pre-chilled 1 X PBS and the cell pellets were snap frozen in liquid nitrogen.

Frozen cell pellets were thawed on ice and resuspended in 500 µl extraction solvent (3:2:1, ACN: MeOH, H_2O). Extraction was performed as previously described (*64*). Samples were injected onto an UltiMate 3000 HPLC system (ThermoFisher Scientific™, Waltham, MA, USA) coupled online to a QTRAP® 5000 mass spectrometer (Sciex, Framingham, USA). Chromatographic separation of GGPP and FPP were performed on a Waters XSelect HSS T3 XP column column (2.5 µm, 2.1 x 150 mm) with 20 mM NH_4HCO_3 and 0.1 % tributylamine in H_2O and ACN:H_2O as mobile phases A and B, respectively. Metabolites were eluted at a constant flow rate of 0.4 ml and linear LC gradient was as follows: 0-2 min 0-20 % B, 2-6 min 20-100 % B, 6-7 min at 100 % B, 7-7.1 min 100-0 % B, 7.1-12 min at 0 % B. Autosampler was kept at 4 °C and column oven was set at 40 °C.

Mass spectrometric measurement was performed in negative ionization mode. For identification and quantitation, a multiple reaction monitoring (MRM) method was used, with specific transitions for every metabolite. Peak areas of all samples and standards for linear regression were determined in Analyst® Software (v. 1.6.2, AB Sciex) and areas for single compounds were exported.

Glycolytic and mitochondrial metabolism analysis

The glycolytic and mitochondrial activity of monocytes was analysed with a Seahorse extracellular flux 96 analyzer (Seahorse Bioscience). The analyzer was operated in a hypoxia box with 1% oxygen and was allowed for at least 24 h to equilibrate at this atmosphere. Cells were seeded without FBS at a density of 4 x 10^5 cells/100 µl RPMI 1640 under normoxic conditions for 30min to get an adherent cell monolayer. Afterwards cells were washed with medium, and finally 180 µl of RPMI 1640 (#R1383 Sigma-Aldrich) containing 5 % FBS, 2 mM glutamine and 5 mM glucose or no glucose was added. The injection ports of the analyzer were filled with RPMI 1640 without FBS containing LPS or the indicated inhibitors. Extracellular acidification rate (ECAR) and oxygen consumption rate (OCR) were determined at 37°C and hypoxic conditions (1 % oxygen).

RNA isolation

1.5 x10^6 monocytes per 1 ml cell culture medium with 5 mM glucose or without glucose (0 mM) were primed with 100 ng/ml LPS in 24-well plates coated with 1.5 % agarose for the indicated time points. After stimulation, the cell suspension was centrifuged at 10000 g for 2 min at 4 °C, the supernatant was removed and the cell pellet was lysed in 400 µl of LYSIS LR buffer from Biotechrabbit. RNA was isolated using the GenUP Total RNA Kit from Biotechrabbit according to the manufacturer's instructions. In brief, the cell lysate was transferred to a DNA mini filter and centrifuged at 12000 g for 2 min at RT. The filtrate obtained was mixed with cold 70 % EtOH (1:1 ratio), placed on an RNA mini filter and centrifuged again at 12000 g for 2 min at RT. The RNA mini filter was washed with 500 µl wash buffer A and 700 µl wash buffer B (12000 g, 1 min, RT). To elute the RNA, 50 µl of RNAase free water was added to the RNA-Mini Filter and centrifuged at 8000 g for 1 min at RT. RNA extraction with Trizol (Invitrogen) was used for deep sequencing and other applications. RNA content and purity were determined using NanoDrop.

Reverse transcriptase-polymerase chain reaction (RT-PCR)

400 ng/ml of the isolated RNA was transcribed into complementary DNA (cDNA) using the TaqMan Reverse Transcription Reagents Kit according to the manufacturer's protocol. For the RT-PCR reaction 1 X RT-Buffer, 1.75 mM MgCl2, 2.5 mM dNTP mix, 50 µl Random hexamer, 1.0 U/µl RNase inhibitor and 2.5 µM MultiScribe^{TM} reverse transcriptase were used.

Real-time Reverse Transcription-polymerase chain reaction (Real-time RT-PCR)

The TaqMan assay from Applied Biosystems was used to quantify the mRNA content of *3-hydroxy-3-methyl-glutaryl-coenzyme A reductase* (*HMGCR*). To calculate the relative differences in mRNA expression of the *HMGCR* under different stimulation conditions, an untreated control (0 h time point) and the reference gene *hypoxanthine phosphoribosyl transferase 1* (*HPRT1*) were used. In addition, a control, without synthesized cDNA, was used to detect possible contamination by foreign DNA. For a 20 µl real time RT-PCR reaction, the 2 X universal master mix, 1 µl cDNA and the 20 X gene expression assays Hs00168352_m1 for HMGCR and Hs02800695_m1 for HPRT1 were used in the Applied Biosystem 7500 real-time PCR instrument according to manufacturer`s protocol. To evaluate the relative content of HMGCR mRNA, the ratio of treated sample to untreated sample was normalized to the reference gene and calculated as $2^{-(\Delta\Delta Ct\ HMGCR)}$.

Quantification and statistical analysis

Prism10 .0, Graph Pad software was used for statistical analysis of data sets. For data with n=3, Student`s unpaired two-tailed t-test was performed. For n > 3, the normal distribution was first checked with the Kolmogorov-Smirnov test and then Student`s unpaired two-tailed t-test or the Student's paired two tailed t-test were used for parametric data and Mann-Whitney U-test was used for non-parametric data. Standard deviation (SD) is presented in all figures displaying normal data distribution, while standard error of the mean (SEM) is shown for non-normally distributed data. The statistical significances are marked as follows: *$p < 0.05$, **$p < 0.01$, *** $p < 0.001$, and ****$p < 0.0001$.

KEY RESOURCES TABLE

Reagent or Resource	Source	Identifier
Antibodies		
anti-ASC	Santa Cruz Biotechnology	Cat# sc-271054
anti-β-Actin	Cell Signaling	Cat# 8457
anti-Cas9	Cell Signaling	Cat# 14697
anti-Caspase-1	Cell Signaling	Cat# 2225
anti-Cryopyrin	Santa Cruz Biotechnology	Cat# sc-66846
anti-GAPDH	Santa Cruz Biotechnology	Cat# sc-32233
anti-IL-1β	Santa Cruz Biotechnologies	Cat# sc-7884
anti-IQGAP1	Cell Signaling	Cat# 20648
anti-mouse IgG, HRP-linked	Cell Signaling	Cat# 7076
anti-NLRP3	Adipogen	Cat# AG-20B-0014-C100
anti-rabbit IgG	Santa Cruz Biotechnology	Cat# sc-2027
anti-rabbit IgG, HRP-linked	Cell Signaling	Cat# 7074
anti-phospho AMPKα T172	Cell Signaling	Cat# 2535
anti-Rac1	Merck	Cat# 05-389
anti-Vinculin	Santa Cruz Biotechnology	Cat# sc-25336

Chemicals, peptides, and recombinant proteins		
Adenosine 5′-triphosphate disodium salt trihydrate (ATP)	Roche	Cat# 10519979001
Agarose	Serva	Cat# 11406.02
AICAR	Tocris	Cat# 2840
Atorvastatin (AS)	Selleckchem	Cat# S5715
Blasticidin	Invivogen	Cat# anti-bl
CHAPS	Carl Roth	Cat# 1479.1
Complete	Merck	Cat# 11836170001
Dehydroepiandrosterone (DHEA)	Cayman Chemical	Cat# Cay15728
Dulbecco′s Phosphate Buffered Saline (DPBS)	Merck	Cat# D8537
Edit-R Lentiviral hEF1α-Blast-Cas9 Nuclease Particles	Dharmacon	Cat# VCAS10126
Edit-R Lentiviral mCMV-Puro MEFV sgRNA particles	Dharmacon	Cat# VSGH10142-246536801
Edit-R Lentiviral mCMV-Puro non-targeting sgRNA particles	Dharmacon	Cat# VSGC10216
EDTA	Merck	Cat# 324503
EHT1864	Tocris	Cat# 3872
Ethanol	AppliChem	Cat# A4230
Farnesyl pyrophosphate ammonium salt (FPP)	Sigma-Aldrich	Cat# F6892
Fetal bovin serum (FBS)	Thermo Fisher Scientific	Cat# 10270098
Ficoll-Paque PLUS	GE Healthcare	Cat# 17-1440-03
Geranylgeranyl pyrophosphate ammonium salt (GGPP)	Sigma-Aldrich	Cat# G6025
GGTI 298	Tocris	Cat# 2430
Glucose	Sigma-Aldrich	Cat# G8644
GlutaMax	Thermo Fisher Scientific	Cat# 35050061
Glycerol	Thermo Fisher Scientific	Cat# 49783
Glycerol 2-phosphate	Merck	Cat# G9422
Hepes	Sigma-Aldrich	Cat# H4034
Hygromycin B Gold	Invivogen	Cat# anti-hg
IGEPAL CA-630	Merck	Cat# I3021
LPS-EB Ultrapure, from E. coli 0111:B4	Invivogen	Cat# tlrl-3peips

Methanol	Merck	Cat# 1060091011
MitoSOX	Thermo Fisher Scientific	Cat# M36006
Monosodium urate crystals (MSU)	Invivogen	Cat# tlrl-msu-25
NP-40	Merck	Cat# 492016
NSC 23766	Santa Cruz Biotechnology	Cat# sc-204823
NuPAGE LDS Sample Buffer	Thermo Fisher Scientific	Cat# NP0007
NuPAGE MES SDS Running Buffer (20X)	Thermo Fisher Scientific	Cat# NP0002
Penicillin/Streptomycin (10,000 U/ml)	Thermo Fisher Scientific	Cat# 15140122
Phorbol-12-myristate-13-acetate (PMA)	Tocris	Cat# 1201
PhosStop	Roche	Cat# 4906845001
Phenylmethanesulfonylfluoride (PMSF)	Sigma-Aldrich	Cat# P7626
Puromycin	Invivogen	Cat# anti-pr
Recombinant human IFN-gamma protein (IFN-γ)	R&D Systems	Cat# 285-IF
RPMI 1640 Medium	Sigma-Aldrich	Cat# R1383
RPMI 1640 Medium	Thermo Fisher Scientific	Cat# 11875085
RPMI Medium, no glucose	Thermo Fisher Scientific	Cat# 11879020
Simvastatin	Tocris	Cat# 1965
siRNA Cryopyrin/NLRP3	Santa Cruz Biotechnology	Cat# sc-45469
siRNA G6PD	Santa Cruz Biotechnology	Cat# sc-60667
siRNA-E (control)	Santa Cruz Biotechnology	Cat# sc-44233
siRNA IQGAP1	Santa Cruz Biotechnology	Cat# sc-35700
siRNA Pyrin	Abbexa	Cat# abx903213
Sodium chlorid	Carl Roth	Cat# 3957.3
Sodium deoxycholate	Thermo Fisher Scientific	Cat# 89904
Sodium dodecylsulfate	Carl Roth	Cat# 2326.2
Sodium orthovanadate	Sigma-Aldrich	Cat# S6508
Squalen (SQ)	Merck	Cat# S3626

Taqman gene expression Assay (FAM), HMGCR	Applied Biosystems, Thermo Fisher Scientific	Cat# 4331182
Taqman gene expression Assay (FAM), HPRT1	Applied Biosystems, Thermo Fisher Scientific	Cat# 4331182
TaqMan 2X Universal PCR Master Mix	Applied Biosystems, Thermo Fisher Scientific	Cat# 4304437
Tris Buffered Saline (TBS)	Merck	Cat# T6664
Tris	AppliChem	Cat# A1086
Triton X-100	Merck	Cat# X100
TWEEN 20	Merck	Cat# 1379
Western Lightning Plus-ECL	PerkinElmer	Cat# NEL104001EA
Zeocin	Invivogen	Cat# ant-zn
6-Aminonicotinamide	Selleckchem	Cat# S9783
Critical commercial assays		
Caspase-Glo 1 Inflammasome Assay	Promega	Cat# G9951
CD11b MicroBeads, human and mouse	Miltenyi Biotec	Cat# 130-049-601
Classical Monocyte Isolation Kit, human	Miltenyi Biotec	Cat# 130-117-337
Detergent Compatibility Assay (DC-Assay)	Bio-Rad	Cat# 5000116
GenUP™ Total RNA Kit	Biotechrabbit, Biozym	Cat# 350700902
Guide-it Mutation Detection Kit	Takara Bio	Cat# 631443
Human 3-hydroxy-3-methyl-glutaryl-coenzyme A reductase (HMGCR) ELISA Kit	My BioSource	Cat# MBS2533319
Human IL-1β ELISA Set II	BD Bioscience	Cat# 557953
Human IL-18 ELISA Kit	Ray-Biotech	Cat# ELH-IL18
Lactate-Dehydrogenase (LDH) Cytotoxicity Assay kit	Pierce	Cat# 88953
Mouse IL-1 β uncoated ELISA Kit	Invitrogen	Cat# 88-7013-88

PicoProbe NADH Quantitation Fluorometric Kit	BioVision	Cat# K338-100
PicoProbe NADPH Quantitation Fluorometric Kit	BioVision	Cat# K349-100
P24 ELISA	Sino Biologicals	Cat# KIT11695
TaqMan™ Reverse Transcription Reagents	Thermo Fisher Scientific	Cat# N8080234
Viromer GREEN	Lipocalyx GmbH	Cat# VG-01LB-03
Deposite data		
Raw metabolomics data		
Raw data from figures		
Experimental models: Organisms/strains		
BALB/c mice	Medizinisch Experimentelles Zentrum, Medical Faculty of the University Leipzig	N/A
C57BL/6J mice	Medizinisch Experimentelles Zentrum, Medical Faculty of the University Leipzig	N/A
DBA mice	Janvier Labs	N/A
THP-1-ASC-GFP	Invivogen	Cat# thp-ascgfp
THP-1 def ASC	Invivogen	Cat# thp-dasc
THP-1 def Caspase-1	Invivogen	Cat# thp-dcasp1
THP-1 def NLRP3	Invivogen	Cat# thp-dnlp
THP-1 def Null	Invivogen	Cat# thp-null
THP-1 DSMZ	DSMZ	Cat# ACC16
Oligonucleotides		
Primers for MEFV sgRNA target site, see method details Crisp/Cas9 knockout of MEFV in THP-1 cells		
Software and algorithms		

CellSens Entry	CellSens software	https://www.olympus-lifescience.com/
GraphPad Prism 10 .0	Graphpad software	https://www.graphpad.com/
ImageJ	ImageJ software	https://imagej.nih.gov/ij/
Seahorse XFE96	Agilent	https://www.agilent.com/

Supplementary Materials

Supplementary Figures S1 to S10

References and Notes

1. P. Sadiku, S. R. Walmsley, Hypoxia and the regulation of myeloid cell metabolic imprinting: consequences for the inflammatory response. *EMBO Rep.* **20**, e47388 (2019).
2. L. A. J. O'Neill, D. Grahame Hardie, Metabolism of inflammation limited by AMPK and pseudo-starvation. *Nature* **493**, 346–355 (2013).
3. C. H. Chang, J. Qiu, D. O'Sullivan, M. D. Buck, T. Noguchi, J. D. Curtis, Q. Chen, M. Gindin, M. M. Gubin, G. J. W. Van Der Windt, E. Tonc, R. D. Schreiber, E. J. Pearce, E. L. Pearce, Metabolic Competition in the Tumor Microenvironment Is a Driver of Cancer Progression. *Cell* **162**, 1229–1241 (2015).
4. P. M. Gubser, G. R. Bantug, L. Razik, M. Fischer, S. Dimeloe, G. Hoenger, B. Durovic, A. Jauch, C. Hess, Rapid effector function of memory CD8+ T cells requires an immediate-early glycolytic switch. *Nat. Immunol.* **14**, 1064–1072 (2013).
5. D. K. Finlay, E. Rosenzweig, L. V. Sinclair, F. C. Carmen, J. L. Hukelmann, J. Rolf, A. A. Panteleyev, K. Okkenhaug, D. A. Cantrell, PDK1 regulation of mTOR and hypoxia-inducible factor 1 integrate metabolism and migration of CD8+ T cells. *J. Exp. Med.* **209**, 2441–2453 (2012).
6. L. Z. Shi, R. Wang, G. Huang, P. Vogel, G. Neale, D. R. Green, H. Chi, HIF1α-dependent glycolytic pathway orchestrates a metabolic checkpoint for the differentiation of TH17 and Treg cells. *J. Exp. Med.* **208**, 1367–1376 (2011).
7. A. N. Macintyre, V. A. Gerriets, A. G. Nichols, R. D. Michalek, M. C. Rudolph, D. Deoliveira, S. M. Anderson, E. D. Abel, B. J. Chen, L. P. Hale, J. C. Rathmell, The glucose transporter Glut1 is selectively essential for CD4 T cell activation and effector function. *Cell Metab.* **20**, 61–72 (2014).
8. K. C. Liao, J. Mogridge, Activation of the Nlrp1b inflammasome by reduction of cytosolic ATP. *Infect. Immun.* **81**, 570–579 (2013).
9. J. Zhao, Y. Mou, J. D. Bernstock, D. Klimanis, S. Wang, M. Spatz, D. Maric, K. Johnson, D. M. Klinman, X. Li, X. Li, J. M. Hallenbeck, Synthetic oligodeoxynucleotides containing multiple telemeric TTAGGG motifs suppress inflammasome activity in macrophages subjected to oxygen and glucose deprivation and reduce ischemic brain injury in stroke-prone spontaneously hypertensive rats. *PLoS*

One **10**, e0140772 (2015).

10. L. E. Sanman, Y. Qian, N. A. Eisele, T. M. Ng, W. A. van der Linden, D. M. Monack, E. Weerapana, M. Bogyo, Disruption of glycolytic flux is a signal for inflammasome signaling and pyroptotic cell death. *Elife* **5**, e0140772 (2016).

11. S. Watanabe, F. Usui-Kawanishi, T. Karasawa, H. Kimura, R. Kamata, T. Komada, Y. Inoue, N. Mise, T. Kasahara, M. Takahashi, Glucose regulates hypoxia-induced NLRP3 inflammasome activation in macrophages. *J. Cell. Physiol.* **235**, 7554–7566 (2020).

12. R. Stienstra, R. T. Netea-Maier, N. P. Riksen, L. A. B. Joosten, M. G. Netea, Specific and Complex Reprogramming of Cellular Metabolism in Myeloid Cells during Innate Immune Responses. *Cell Metab.* **26**, 142–156 (2017).

13. B. Everts, E. Amiel, S. C. C. Huang, A. M. Smith, C. H. Chang, W. Y. Lam, V. Redmann, T. C. Freitas, J. Blagih, G. J. W. Van Der Windt, M. N. Artyomov, R. G. Jones, E. L. Pearce, E. J. Pearce, TLR-driven early glycolytic reprogramming via the kinases TBK1-IKKε supports the anabolic demands of dendritic cell activation. *Nat. Immunol.* **15**, 323–332 (2014).

14. L. A. J. O'Neill, E. J. Pearce, Immunometabolism governs dendritic cell and macrophage function. *J. Exp. Med.* **213**, 15–23 (2016).

15. G. M. Tannahill, A. M. Curtis, J. Adamik, E. M. Palsson-Mcdermott, A. F. McGettrick, G. Goel, C. Frezza, N. J. Bernard, B. Kelly, N. H. Foley, L. Zheng, A. Gardet, Z. Tong, S. S. Jany, S. C. Corr, M. Haneklaus, B. E. Caffrey, K. Pierce, S. Walmsley, F. C. Beasley, E. Cummins, V. Nizet, M. Whyte, C. T. Taylor, H. Lin, S. L. Masters, E. Gottlieb, V. P. Kelly, C. Clish, P. E. Auron, R. J. Xavier, L. A. J. O'Neill, Succinate is an inflammatory signal that induces IL-1β through HIF-1α. *Nature* **496**, 238–242 (2013).

16. A. Haschemi, P. Kosma, L. Gille, C. R. Evans, C. F. Burant, P. Starkl, B. Knapp, R. Haas, J. A. Schmid, C. Jandl, S. Amir, G. Lubec, J. Park, H. Esterbauer, M. Bilban, L. Brizuela, J. A. Pospisilik, L. E. Otterbein, O. Wagner, The sedoheptulose kinase CARKL directs macrophage polarization through control of glucose metabolism. *Cell Metab.* **15**, 813–826 (2012).

17. N. Raulien, K. Friedrich, S. Strobel, S. Rubner, S. Baumann, M. von Bergen, A. Körner, M. Krueger, M. Rossol, U. Wagner, Fatty acid oxidation compensates for lipopolysaccharide-induced Warburg effect in glucose-deprived monocytes. *Front. Immunol.* **8**, 609 (2017).

18. P. Newsholme, R. Curi, S. Gordon, E. A. Newsholme, Metabolism of glucose, glutamine, long-chain fatty acids and ketone bodies by murine macrophages. *Biochem. J.* **239**, 121–125 (1986).

19. S. Chettimada, R. Gupte, D. Rawat, S. A. Gebb, I. F. McMurtry, S. A. Gupte, Hypoxia-induced glucose-6-phosphate dehydrogenase overexpression and -activation in pulmonary artery smooth muscle cells: Implication in pulmonary hypertension. *Am. J. Physiol. - Lung Cell. Mol. Physiol.* **308**, L287–L300 (2015).

20. Y. T. Wang, A. J. Trzeciak, W. S. Rojas, P. Saavedra, Y. T. Chen, R. Chirayil, J. I. Etchegaray, C. D. Lucas, D. J. Puleston, K. R. Keshari, J. S. A. Perry, Metabolic adaptation supports enhanced macrophage efferocytosis in limited-oxygen environments. *Cell Metab.* **35**, 316-331.e6 (2023).

21. S. H. L. Mandey, L. M. Kuijk, J. Frenkel, H. R. Waterham, A role for

geranylgeranylation in interleukin-1β secretion. *Arthritis Rheum.* **54**, 3690–3695 (2006).

22. M. T. Montero, O. Hernández, Y. Suárez, J. Matilla, A. J. Ferruelo, J. Martínez-Botas, D. Gómez-Coronado, M. A. Lasunción, Hydroxymethylglutaryl-coenzyme A reductase inhibition stimulates caspase-1 activity and Th1-cytokine release in peripheral blood mononuclear cells. *Atherosclerosis* **153**, 303–313 (2000).

23. P. A. Kiener, P. M. Davis, J. L. Murray, S. Youssef, B. M. Rankin, M. Kowala, Stimulation of inflammatory responses in vitro and in vivo by lipophilic HMG-CoA reductase inhibitors. *Int. Immunopharmacol.* **1**, 105–118 (2001).

24. W. R. Coward, A. Marei, A. Yang, M. M. Vasa-Nicotera, S. C. Chow, Statin-Induced Proinflammatory Response in Mitogen-Activated Peripheral Blood Mononuclear Cells through the Activation of Caspase-1 and IL-18 Secretion in Monocytes. *J. Immunol.* **176**, 5284–5292 (2006).

25. S. Bekkering, R. J. W. Arts, B. Novakovic, I. Kourtzelis, C. D. C. C. van der Heijden, Y. Li, C. D. Popa, R. ter Horst, J. van Tuijl, R. T. Netea-Maier, F. L. van de Veerdonk, T. Chavakis, L. A. B. Joosten, J. W. M. van der Meer, H. Stunnenberg, N. P. Riksen, M. G. Netea, Metabolic Induction of Trained Immunity through the Mevalonate Pathway. *Cell* **172**, 135-146.e9 (2018).

26. I. Mitroulis, K. Ruppova, B. Wang, L. S. Chen, M. Grzybek, T. Grinenko, A. Eugster, M. Troullinaki, A. Palladini, I. Kourtzelis, A. Chatzigeorgiou, A. Schlitzer, M. Beyer, L. A. B. Joosten, B. Isermann, M. Lesche, A. Petzold, K. Simons, I. Henry, A. Dahl, J. L. Schultze, B. Wielockx, N. Zamboni, P. Mirtschink, Ü. Coskun, G. Hajishengallis, M. G. Netea, T. Chavakis, Modulation of Myelopoiesis Progenitors Is an Integral Component of Trained Immunity. *Cell* **172**, 147-161.e12 (2018).

27. J. Moral-Sanz, S. A. Lewis, S. MacMillan, F. A. Ross, A. Thomson, B. Viollet, M. Foretz, C. Moran, D. G. Hardie, A. M. Evans, The LKB1–AMPK-1 signaling pathway triggers hypoxic pulmonary vasoconstriction downstream of mitochondria. *Sci. Signal.* **11**, eaau0296 (2018).

28. P. T. Mungai, G. B. Waypa, A. Jairaman, M. Prakriya, D. Dokic, M. K. Ball, P. T. Schumacker, Hypoxia Triggers AMPK Activation through Reactive Oxygen Species-Mediated Activation of Calcium Release-Activated Calcium Channels. *Mol. Cell. Biol.* **31**, 3531–3545 (2011).

29. F. Dengler, R. Rackwitz, H. Pfannkuche, G. Gäbel, Glucose transport across lagomorph jejunum epithelium is modulated by AMP-activated protein kinase under hypoxia. *J. Appl. Physiol.* **123**, 1487–1500 (2017).

30. T. Hashimoto, Y. Murata, Y. Urushihara, S. Shiga, K. Takeda, Y. Hosoi, Severe hypoxia increases expression of ATM and DNA-PKcs and it increases their activities through Src and AMPK signaling pathways. *Biochem. Biophys. Res. Commun.* **505**, 13–19 (2018).

31. D. Carling, P. R. Clarke, V. A. Zammit, D. G. Hardie, Purification and characterization of the AMP-activated protein kinase: Copurification of acetyl-CoA carboxylase kinase and 3-hydroxy-3-methylglutaryl-CoA reductase kinase activities. *Eur. J. Biochem.* **186**, 129–136 (1989).

32. J. Ecker, G. Liebisch, M. Englmaier, M. Grandl, H. Robenek, G. Schmitz, Induction of fatty acid synthesis is a key requirement for phagocytic differentiation of human monocytes. *Proc. Natl. Acad. Sci. U. S. A.* **107**, 7817–7822 (2010).

33. A. D. Nguyen, J. G. McDonald, R. K. Bruick, R. A. DeBose-Boyd, Hypoxia stimulates degradation of 3-hydroxy-3-methylglutaryl-coenzyme A reductase through accumulation of lanosterol and hypoxia-inducible factor-mediated induction of insigs. *J. Biol. Chem.* **282**, 27436–27446 (2007).

34. P. Kucharzewska, H. C. Christianson, M. Belting, Global profiling of metabolic adaptation to hypoxic stress in human glioblastoma cells. *PLoS One* **10**, e0116740 (2015).

35. J. Luo, H. Yang, B. L. Song, Mechanisms and regulation of cholesterol homeostasis. *Nat. Rev. Mol. Cell Biol.* **21**, 225–245 (2020).

36. L. M. Kuijk, J. M. Beekman, J. Koster, H. R. Waterham, J. Frenkel, P. J. Coffer, HMG-CoA reductase inhibition induces IL-1beta release through Rac1/PI3K/PKB-dependent caspase-1 activation. *Blood* **112**, 3563–3573 (2008).

37. J. Jin, H. Qian, B. Wan, L. Zhou, C. Chen, Y. Lv, M. Chen, S. Zhu, L. Ye, X. Wang, W. Xu, T. Lv, Y. Song, Geranylgeranyl diphosphate synthase deficiency hyperactivates macrophages and aggravates lipopolysaccharide-induced acute lung injury. *Am. J. Physiol. - Lung Cell. Mol. Physiol.* **320**, L1011–L1024 (2021).

38. Y. H. Park, G. Wood, D. L. Kastner, J. J. Chae, Pyrin inflammasome activation and RhoA signaling in the autoinflammatory diseases FMF and HIDS. *Nat. Immunol.* **17**, 914–921 (2016).

39. M. K. Akula, M. Shi, Z. Jiang, C. E. Foster, D. Miao, A. S. Li, X. Zhang, R. M. Gavin, S. D. Forde, G. Germain, S. Carpenter, C. V. Rosadini, K. Gritsman, J. J. Chae, R. Hampton, N. Silverman, E. M. Gravallese, J. C. Kagan, K. A. Fitzgerald, D. L. Kastner, D. T. Golenbock, M. O. Bergo, D. Wang, Control of the innate immune response by the mevalonate pathway. *Nat. Immunol.* **17**, 922–929 (2016).

40. B. D. Henriksbo, A. K. Tamrakar, J. S. Phulka, N. G. Barra, J. D. Schertzer, Statins activate the NLRP3 inflammasome and impair insulin signaling via p38 and mTOR. *Am. J. Physiol. - Endocrinol. Metab.* **319**, E110–E116 (2020).

41. O. P. Skinner, J. Jurczyluk, P. J. Baker, S. L. Masters, A. G. Rios Wilks, M. S. Clearwater, A. A. B. Robertson, K. Schroder, S. Mehr, M. A. Munoz, M. J. Rogers, Lack of protein prenylation promotes NLRP3 inflammasome assembly in human monocytes. *J. Allergy Clin. Immunol.* **143**, 2315-2317.e3 (2019).

42. Y.-H. Liao, Y.-C. Lin, S.-T. Tsao, Y.-C. Lin, A.-J. Yang, C.-T. Huang, K.-C. Huang, W. W. Lin, HMG-CoA reductase inhibitors activate caspase-1 in human monocytes depending on ATP release and P2X7 activation. *J. Leukoc. Biol.* **93**, 289–299 (2013).

43. R. Van Der Burgh, K. Pervolaraki, M. Turkenburg, H. R. Waterham, J. Frenkel, A. M. Boes, Unprenylated RhoA contributes to IL-1 β hypersecretion in mevalonate kinase deficiency model through stimulation of Rac1 activity. *J. Biol. Chem.* **289**, 27757–27765 (2014).

44. J. N. Ibrahim, R. Jounblat, N. Jalkh, J. Abou Ghoch, C. Al Hageh, E. Chouery, A. Mégarbané, J. C. Lecron, M. Medlej-Hashim, RAC1 expression and role in IL-1β production and oxidative stress generation in familial Mediterranean fever (FMF) patients. *Eur. Cytokine Netw.* **29**, 127–135 (2018).

45. Q. Zhang, S. M. Conley, G. Li, X. Yuan, P. L. Li, Rac1 GTPase Inhibition Blocked Podocyte Injury and Glomerular Sclerosis during Hyperhomocysteinemia via Suppression of Nucleotide-Binding Oligomerization Domain-Like Receptor Containing Pyrin Domain 3 Inflammasome Activation. *Kidney Blood Press. Res.* **44**,

513–532 (2019).

46. C. Ying, Z. Zhou, J. Dai, M. Wang, J. Xiang, D. Sun, X. Zhou, Activation of the NLRP3 inflammasome by RAC1 mediates a new mechanism in diabetic nephropathy. *Inflamm. Res.* **71**, 191–204 (2022).

47. O. M. Khan, M. X. Ibrahim, I. M. Jonsson, C. Karlsson, M. Liu, A. K. M. Sjogren, F. J. Olofsson, M. Brisslert, S. Andersson, C. Ohlsson, L. M. Hultén, M. Bokarewa, M. O. Bergo, Geranylgeranyltransferase type I (GGTase-I) deficiency hyperactivates macrophages and induces erosive arthritis in mice. *J. Clin. Invest.* **121**, 628–639 (2011).

48. M. K. Akula, M. X. Ibrahim, E. G. Ivarsson, O. M. Khan, I. T. Kumar, M. Erlandsson, C. Karlsson, X. Xu, M. Brisslert, C. Brakebusch, D. Wang, M. Bokarewa, V. I. Sayin, M. O. Bergo, Protein prenylation restrains innate immunity by inhibiting Rac1 effector interactions. *Nat. Commun.* **10**, 3975 (2019).

49. J. L. Larson-Casey, M. Vaid, L. Gu, C. He, G. Q. Cai, Q. Ding, D. Davis, T. F. Berryhill, L. S. Wilson, S. Barnes, J. D. Neighbors, R. J. Hohl, K. A. Zimmerman, B. K. Yoder, A. L. F. Longhini, V. S. Hanumanthu, R. Surolia, V. B. Antony, A. Brent Carter, Increased flux through the mevalonate pathway mediates fibrotic repair without injury. *J. Clin. Invest.* **129**, 4962–4978 (2019).

50. R. X. Leng, D. S. Di, J. Ni, X. X. Wu, L. L. Zhang, X. F. Wang, R. S. Liu, Q. Huang, Y. G. Fan, H. F. Pan, B. Wang, D. Q. Ye, Identification of new susceptibility loci associated with rheumatoid arthritis. *Ann. Rheum. Dis.* **79**, 1565–1571 (2020).

51. H. J. I. De Jong, O. H. Klungel, L. Van Dijk, R. J. Vandebriel, H. G. M. Leufkens, J. W. Van Der Laan, J. W. Cohen Tervaert, H. Van Loveren, Use of statins is associated with an increased risk of rheumatoid arthritis. *Ann. Rheum. Dis.* **71**, 648–654 (2012).

52. R. J. Vandebriel, H. J. I. De Jong, E. R. Gremmer, O. H. Klungel, J. W. C. Tervaert, W. Slob, J. W. Van Der Laan, H. Van Loveren, Statins accelerate the onset of collagen type II-induced arthritis in mice. *Arthritis Res. Ther.* **14**, R90 (2012).

53. J. R. F. Abreu, W. Dontje, S. Krausz, D. de Launay, P. B. van Hennik, A. M. van Stalborch, J. P. ten Klooster, M. E. Sanders, K. A. Reedquist, M. J. Vervoordeldonk, P. L. Hordijk, P. P. Tak, A Rac1 inhibitory peptide suppresses antibody production and paw swelling in the murine collagen-induced arthritis model of rheumatoid arthritis. *Arthritis Res. Ther.* **12**, R2 (2010).

54. S. Zhu, P. Lu, H. Liu, P. Chen, Y. Wu, Y. Wang, H. Sun, X. Zhang, Q. Xia, B. C. Heng, Y. Zhou, H. W. Ouyang, Inhibition of Rac1 activity by controlled release of NSC23766 from chitosan microspheres effectively ameliorates Osteoarthritis development in vivo. *Ann. Rheum. Dis.* **74**, 285–293 (2015).

55. A. Chan, M. Akhtar, M. Brenner, Y. Zheng, P. S. Gulko, M. Symons, The GTPase Rac regulates the proliferation and invasion of fibroblast-like synoviocytes from rheumatoid arthritis patients. *Mol. Med.* **13**, 297–304 (2007).

56. I. Tiede, G. Fritz, S. Strand, D. Poppe, R. Dvorsky, D. Strand, H. A. Lehr, S. Wirtz, C. Becker, R. Atreya, J. Mudter, K. Hildner, B. Bartsch, M. Holtmann, R. Blumberg, H. Walczak, H. Iven, P. R. Galle, M. R. Ahmadian, M. F. Neurath, CD28-dependent Rac1 activation is the molecular target of azathioprine in primary human CD4+ T lymphocytes. *J. Clin. Invest.* **111**, 1133–1145 (2003).

57. K. Gaffney, D. G. I. Scott, Azathioprine and cyclophosphamide in the treatment of rheumatoid arthritis. *Br. J. Rheumatol.* **37**, 824–836 (1998).

58. K. E. Wellen, G. Hatzivassiliou, U. M. Sachdeva, T. V. Bui, J. R. Cross, C. B. Thompson, ATP-citrate lyase links cellular metabolism to histone acetylation. *Science (80-.).* **324**, 1076–1080 (2009).

59. M. J. MacDonald, M. J. Longacre, S. W. Stoker, M. Kendrick, A. Thonpho, L. J. Brown, N. M. Hasan, S. Jitrapakdee, T. Fukao, M. S. Hanson, L. A. Fernandez, J. Odorico, Differences between human and rodent pancreatic islets: Low pyruvate carboxylase, ATP citrate lyase, and pyruvate carboxylation and high glucose-stimulated acetoacetate in human pancreatic islets. *J. Biol. Chem.* **286**, 18383–18396 (2011).

60. P. R. Hesker, M. T. Nguyen, M. Kovarova, J. P. Y. Ting, B. H. Koller, Genetic Loss of Murine Pyrin, the Familial Mediterranean Fever Protein, Increases Interleukin-1β Levels. *PLoS One* **7** (2012).

61. G. Manukyan, R. Aminov, Update on pyrin functions and mechanisms of familial mediterranean fever. *Front. Microbiol.* **7** (2016).

62. M. Karimov, M. Schulz, T. Kahl, S. Noske, M. Kubczak, I. Gockel, R. Thieme, T. Büch, A. Reinert, M. Ionov, M. Bryszewska, H. Franke, U. Krügel, A. Ewe, A. Aigner, Tyrosine-modified linear PEIs for highly efficacious and biocompatible siRNA delivery in vitro and in vivo: LP10Y for therapeutic siRNA delivery. *Nanomedicine Nanotechnology, Biol. Med.* **36** (2021).

63. K. Murugesan, S. Baumann, D. K. Wissenbach, S. Kliemt, S. Kalkhof, W. Otto, I. Mögel, T. Kohajda, M. von Bergen, J. M. Tomm, Subtoxic and toxic concentrations of benzene and toluene induce Nrf2-mediated antioxidative stress response and affect the central carbon metabolism in lung epithelial cells A549. *Proteomics* **13**, 3211–3221 (2013).

64. J. L. Krause, S. S. Schaepe, K. Fritz-Wallace, B. Engelmann, U. Rolle-Kampczyk, S. Kleinsteuber, F. Schattenberg, Z. Liu, S. Mueller, N. Jehmlich, M. Von Bergen, G. Herberth, Following the community development of SIHUMIx–a new intestinal in vitro model for bioreactor use. *Gut Microbes* **11**, 1116–1129 (2020).

Acknowledgments:

We thank Cornelia Arnold for excellent technical assistance.

Funding:

This work was supported by the German Research Foundation (DFG) (WA 2765/10-1 and WA 2765/5-1 to UW, RO 4037/3-1 to MR) and the Bundesministerium für Forschung und Bildung (BMBF, IFB Adipositas Erkrankungen). MvB is thankful for funding by the DFG (CRC 1052 Mechanisms of Obesity project number 209933838 (B2 and Z3) and for funding by the UFZ for the ProMetheus platform for proteomics and metabolomics.

Author contributions:

Conceptualization: UW, MR

Experiments: NR, KF, SS, SR, KFW, SB, FH, URK, AE, ES

Resources: MP, EL, TK, MvB, MC, AE, AA, GS

Visualization: KF, NR

Supervision: UW, MR

Funding acquisition: UW, MR

Writing – original draft: UW

Writing – review & editing: UW, MR, KF, NR, MP, MvB, MC, ES AE, AA, GS

The order of the shared first authorship was determined by a coin toss. Both NR and KF contributed equally and have the right to list their name first in their CV. All authors have read and approved the final version of the manuscript.

Competing interests: Authors declare that they have no competing interests.

Data and materials availability: All data are available in the main text or the supplementary materials. Further information and requests for resources and reagents should be directed to the lead contact, Prof. Dr. Ulf Wagner (Ulf.Wagner@medizin.uni-leipzig.de). The CRISPR/Cas9 knockout of MEFV THP1 cells generated in this study are available from the lead contact upon reasonable request.

Figure Legends:

Figure 1.

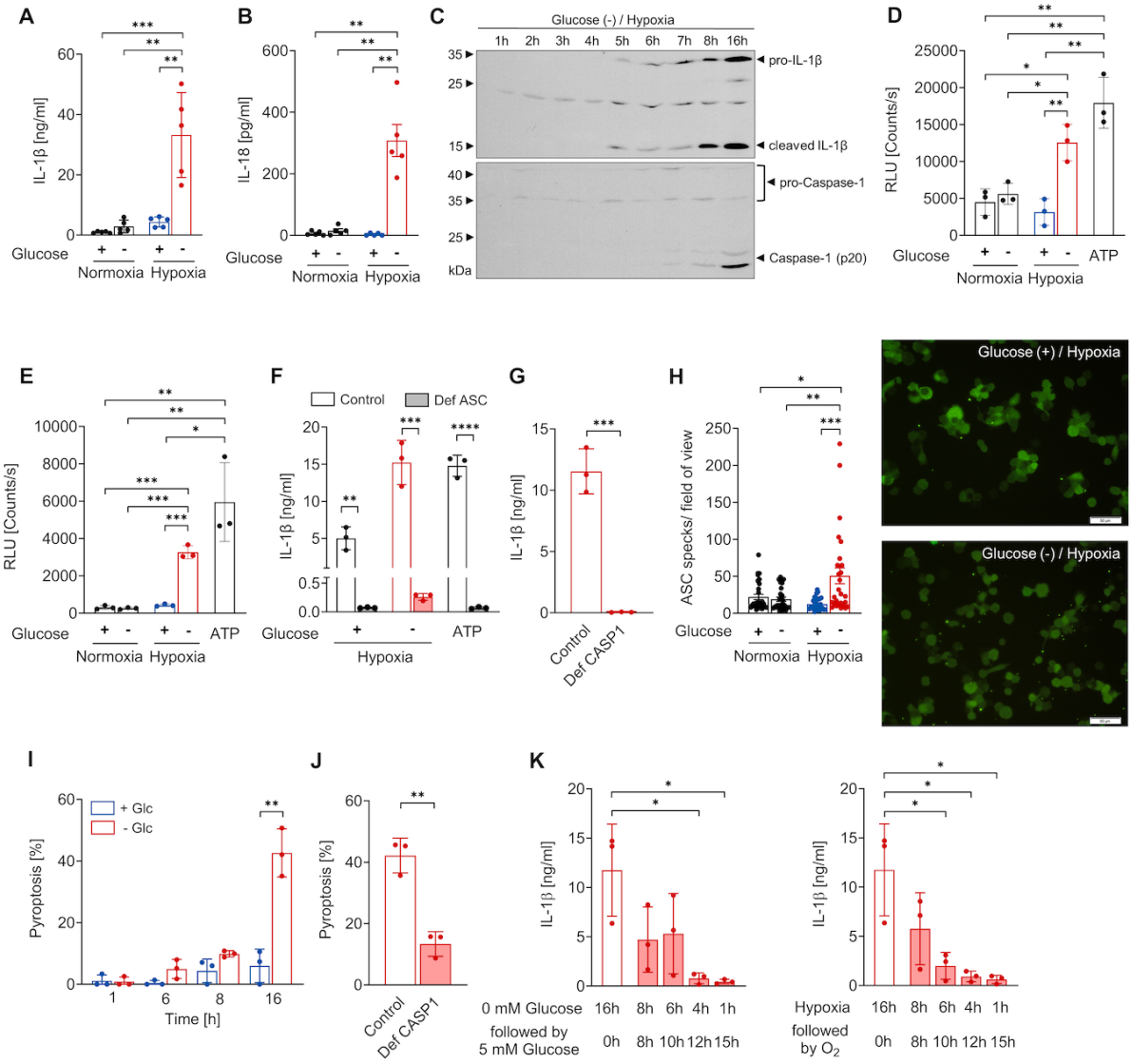

Figure 1. Glucose deprivation under hypoxia induces inflammasome assembly and IL-1β release in monocytes

(**A** and **B**) Detection of IL-1β (A, n=5) and IL-18 (B, n=5) in supernatant of monocytes incubated under indicated conditions (glucose deprivation+hypoxia in red, glucose+hypoxia in blue) for 16 h.

(**C**) Western blot analysis of IL-1β and caspase-1 in the supernatant of monocytes under glucose deprivation and hypoxia. One representative experiment of 3 is shown.

(**D** and **E**) Detection of active caspase-1 in cell lysates (**D**) and supernatant (**E**) of monocytes under indicated conditions for 16h (n=3).

(**F**) IL-1β release of THP-1 cells deficient for ASC (Def ASC) and control cells under indicated conditions for 16 h. ATP was used as control, (n=3).

(**G**) IL-1β release of THP-1 cells deficient for caspase-1 (Def CASP1) and control cells under oxygen and glucose deprivation after 16h (n=3).

(**H**) Quantification of ASC specks in THP-1 ASC-GFP reporter cells after 8h of incubation under the indicated conditions. Each dot represents number of ASC specks from one high power field from 3 experiments. On the right, representative images from 3 replicates. Scale bar, 50 µm.

(**I** and **J**) Rate of pyroptosis under hypoxia in monocytes at the indicated time points (I, n=3) and in caspase-1 deficient (Def CASP1) or control cells after 16h (J, n=3).

(**K**) IL-1β release induced by glucose-oxygen deprivation followed by re-addition of glucose (left) or re-oxygenation (right) at the indicated time points (n=3).
Bars represent mean ± SD (A, D-G and I-K) or ± SEM (B, H), *p < 0.05, **p < 0.01, ***p < 0.001, by Student's unpaired two-tailed t test (A, D-G and I-K) or Mann-Whitney U test (B, H). Each dot represents a single biological replicate

Figure 2.

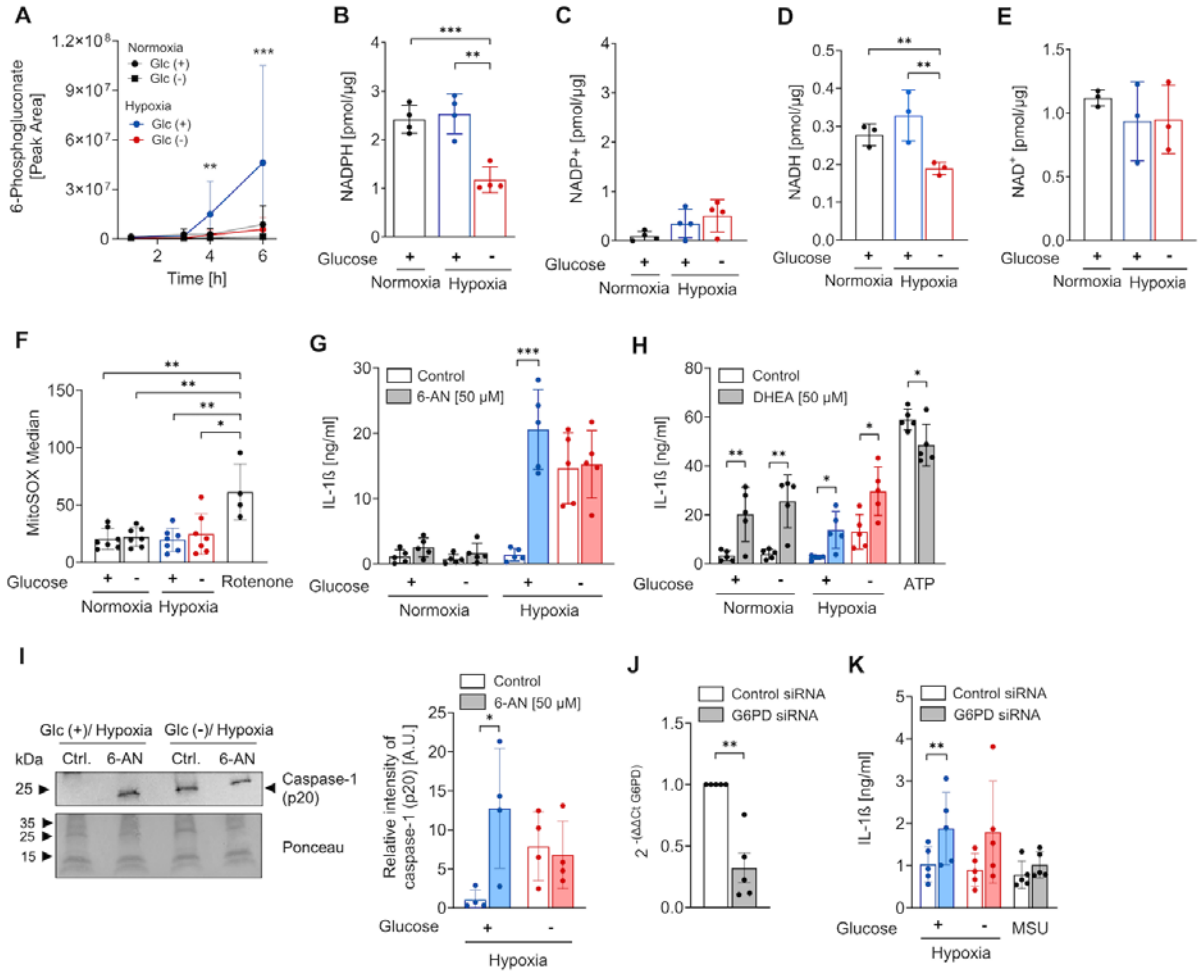

Figure 2. Glucose deprivation under hypoxia decreases 6-phosphogluconate and NADPH generation

(**A**) Concentration of 6-phosphogluconate (peak area) in monocytes under the indicated conditions after 6h (n=7, 3 donors).

(**B** to **E**) Intracellular concentrations of NADPH, NADP+, NADH and NAD+ determined after 6h under indicated conditions (n=4)

(**F**) Detection of mitochondrial reactive oxygen species (mtROS) with MitoSOX (Median) under indicated conditions after 6h (n=7). Rotenone (10 µM) was used as control (n=4).

(**G** and **H**) IL-1β release of monocytes incubated under the indicated conditions for 16h after addition of the inhibitors 6-aminonicotinamide (6-AN, G, n=5) or dehydroepiandrosterone (DHEA, H, n=5) in comparison to controls.

(**I**) Western blot analysis and quantification of caspase-1 in the supernatant of monocytes under indicated conditions after addition of the inhibitor 6-aminonicotinamide (6-AN, n=4). Ponceau staining was used as loading control.

(**J**) Quantification of *glucose-6-phosphate dehydrogenase-(G6PD)* mRNA of monocytes transfected with siRNA specific for G6PD and a control siRNA (n=5).

(**K**) IL-1β release of monocytes transfected with siRNA specific for *G6PD*, and a control siRNA incubated under the indicated conditions for 8h (n=5).

Bars represent mean± SD (B-I, K) or ± SEM (A, J), *p < 0.05, **p < 0.01, ***p < 0.001, by ratio paired t-test (A, K), Student's unpaired two-tailed t test (B, D, F-I), Mann-Whitney U test (J). Each dot represents a single biological replicate.

Figure 3.

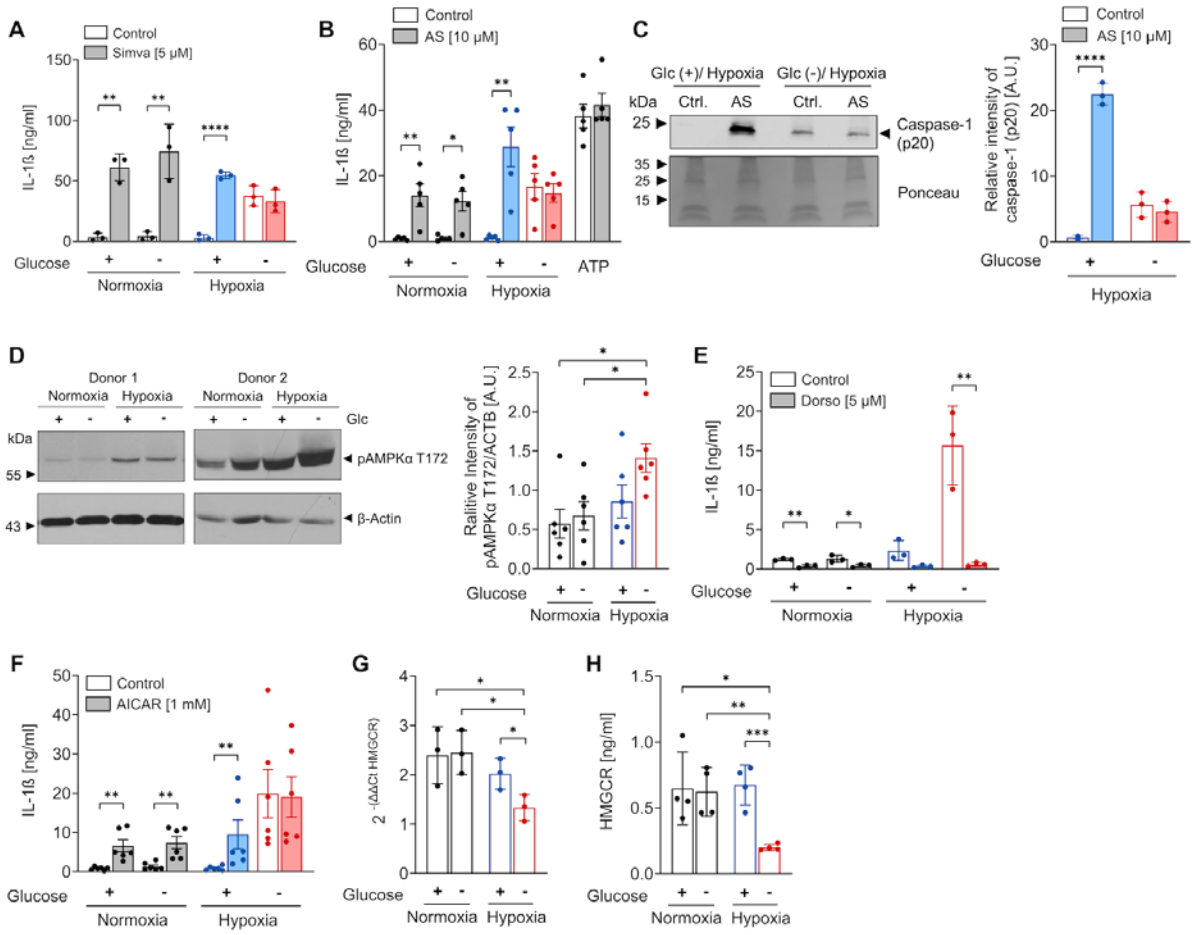

Figure 3: Inhibition of mevalonate kinase pathway and activation of AMPK activate caspase-1

(**A** and **B**) IL-1β release of monocytes incubated under the indicated conditions for 16h after addition of the inhibitors simvastatin (Simva, **A**, n=3) or atorvastatin (AS, **B**, n=5) in comparison to controls.

(**C**) Western blot analysis and quantification of caspase-1 in the supernatant of monocytes under indicated conditions after addition of atorvastatin (AS, n=3). Ponceau staining was used as loading control.

(**D**) Representative Western blots of AMPKα phosphorylation at Threonin 172 (pAMPKα T172) in lysates of monocytes after 2h of incubation under the indicated conditions. β-actin was used as loading control. Bar chart depicts quantification of pAMPKα T172 normalized to β-Actin (n=6).

(**E** and **F**) IL-1β release of monocytes incubated under the indicated conditions for 16h after addition of the AMPK inhibitor dorsomorphin (Dorso, E, n=3) or the AMPK activator AICAR (F, n=6).

(**G** and **H**) Quantification of mRNA (G) and protein content (H) of HMGCR of monocytes stimulated for 2h under the indicated conditions (n=3).

Bars represent mean ± SD (A, C, E, G, I) or ± SEM (B, D, F), *p < 0.05, **p < 0.01, ***p < 0.001, byStudent's unpaired two-tailed t test (A, C, E, G, H) or Mann-Whitney U test (B,D,F). Each dot represents a single biological replicate.

Figure 4.

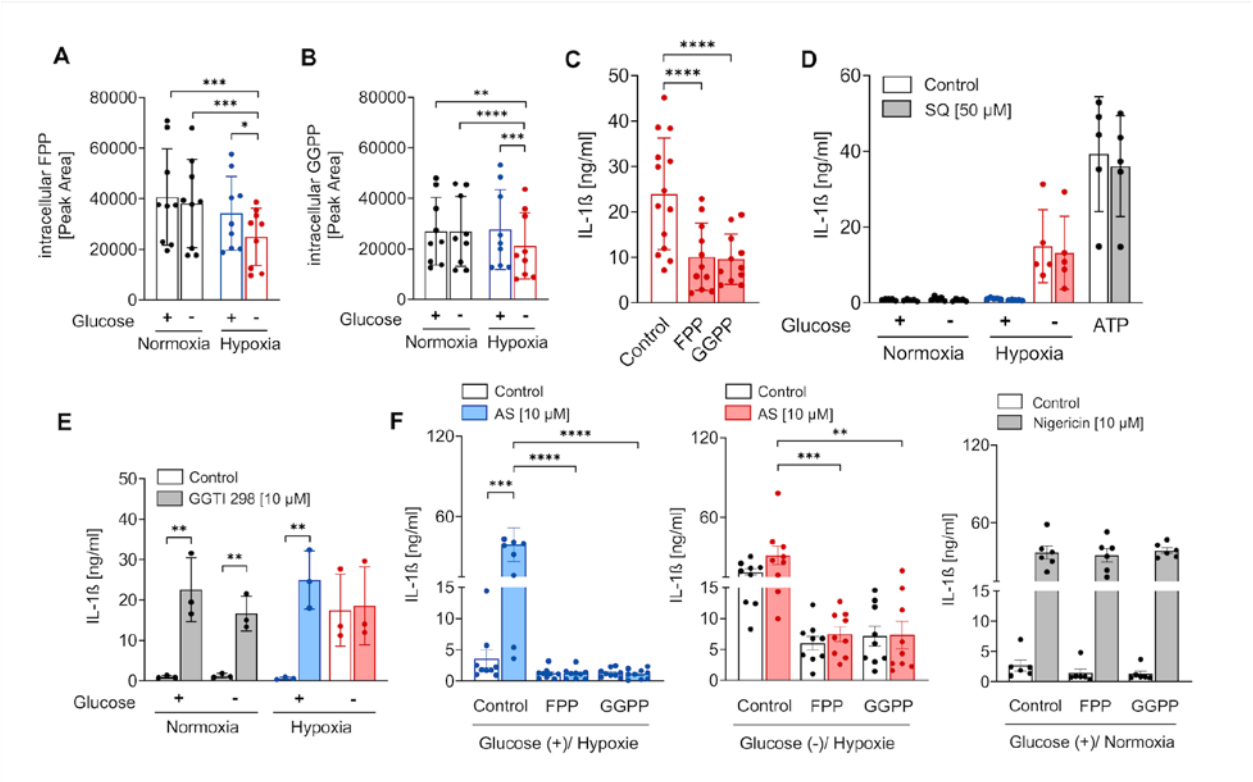

Figure 4. GGPP deficiency activates the NLRP3 inflammasome

(**A** and **B**) Intracellular farnesyl pyrophosphate (FFP, **A**) and geranylgeranyl pyrophosphate (GGPP, **B**) concentrations (peak area) in lysates of monocytes primed with LPS for 6h under the indicated conditions (n=9).

(**C**) IL-1β release of monocytes incubated under glucose-oxygen deprivation in the presence of exogenous FPP (20µM) or GGPP (20µM) supplementation compared to controls for 16h (n=11).

(**D**) IL-ß release of monocytes incubated under indicated conditions in presence of exogenous Squalen (SQ) supplementation or without (control) for 16h (n=5).

(**E**) IL-1β release of monocytes incubated under the indicated conditions for 16h in the presence of the GGTase-I inhibitor GGTI 298 compared to controls (n=3).

(**F**) IL-1ß release of monocytes incubated under indicated conditions in cultures with the HMGCR inhibitor atorvastatin (AS) or without (control) supplemented with exogenous FPP (20µM) or GGPP (20µM) compared to control for 16h (n=6). Nigericin was used as positive control.

Bars represent mean ± SD (A-E) or ± SEM (F), *p < 0.05, **p < 0.01, ***p < 0.001, ****p < 0.0001, by ratio paired t-test (A-C), Student's unpaired two-tailed t test (E) or Mann-Whitney U test (F). Each dot represents a single biological replicate unless indicated otherwise.

Figure 5.

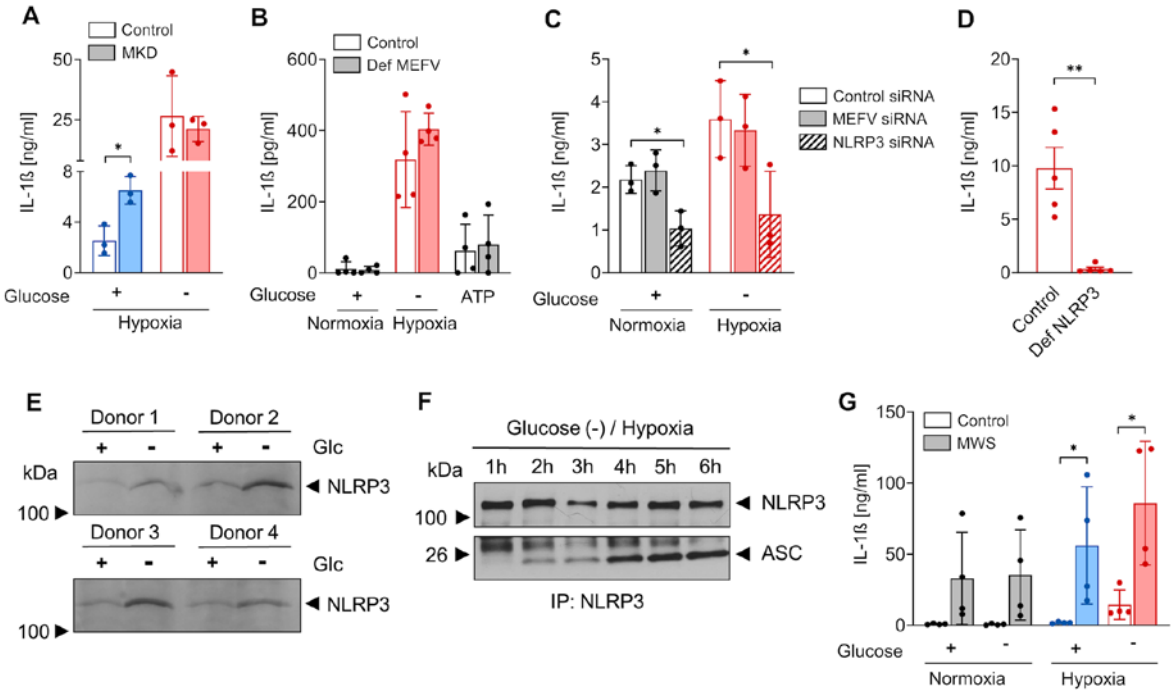

Figure 5. Influence of mevalonate kinase deficiency (MKD) on NLRP3 activation under Glucose deficiency and hypoxia

(**A**) IL-1β release of monocytes incubated for 16h under the indicated conditions from patients with mevalonate kinase deficiency (MKD) compared to their heterozygous mothers (control) (n=3).

(**B**) IL-1β release of pyrin deficient (Def MEFV) and control THP1 cells incubated under glucose-oxygen deprivation compared to control conditions and to ATP stimulation for 8h (n=4).

(**C**) IL-1β release of monocytes transfected with siRNA specific for pyrin (MEFV), NLRP3, and a control siRNA incubated under the indicated conditions for 8h (n=3).

(**D**) IL-1β release of THP-1 cells deficient for NLRP3 (Def NLRP3) compared to control cells (n=5).

(**E**) Western blot analysis of NLRP3 in the supernatant of monocytes incubated under hypoxia for 16h (n=4).

(**F**) Immune precipitation of NLRP3 and detection of bound ASC in lysates of monocytes incubated under glucose-oxygen deprivation at the indicated time points. Shown is one representative experiment out of 3 with 2 donors.

(**G**) IL-1β release of monocytes incubated for 16h under the indicated conditions from patients with Muckle-Wells syndrome (MWS) compared to healthy controls. Shown are results from 4 experiments with monocytes from 2 patients (MWS) in comparison to 4 age-matched healthy controls.

Bars represent mean ± SD (A-C,G) or ± SEM (D), *p < 0.05, **p < 0.01, ***p < 0.001, ****p < 0.0001, by Student's unpaired two-tailed t test (A,C,G) or Mann-Whitney U test (D). Each dot represents a single biological replicate unless indicated otherwise.

Figure 6.

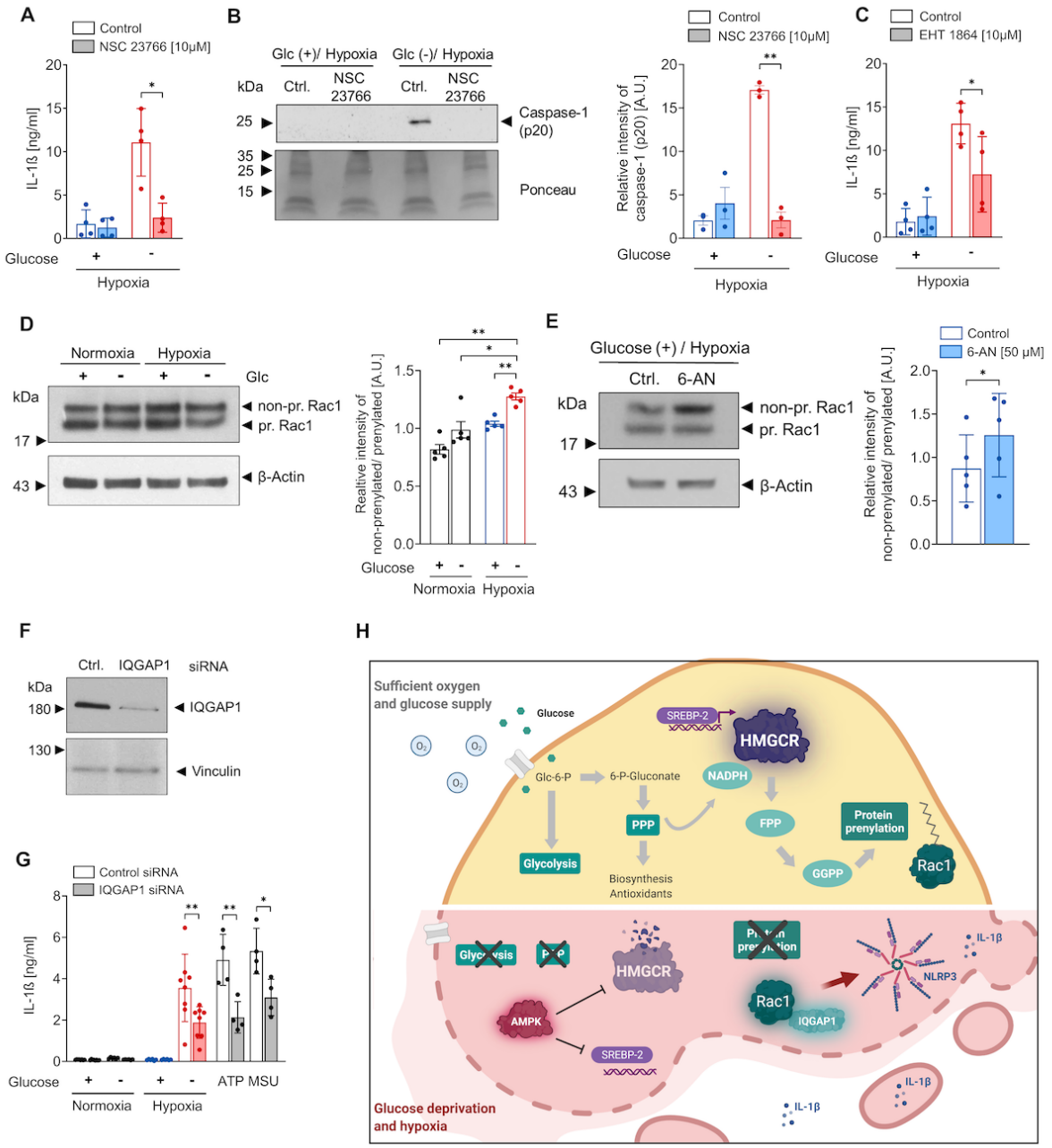

Figure 6: Glucose-oxygen deprivation-induced NLRP3 activation is mediated by interaction between non-prenylated Rac1 and IQGAP1

(**A**) IL-1 β release of monocytes incubated for 16h under hypoxia in the presence of the Rac1 inhibitor NSC 23766 compared to controls (n=3).

(**B**) Western blot analysis and quantification of caspase-1 in the supernatant of monocytes under indicated conditions in the presence of NSC 23766 for 16h compared to controls (n=3). Ponceau staining was used as loading control.

(**C**) IL-1 β release of monocytes incubated for 16h under hypoxia in the presence of the Rac1 inhibitor EHT 1864 compared to controls (n=3).

(**D** and **E**) Western blot analysis of the prenylated (pr.) and non-prenylated (non-pr.) Rac1 in lysates from monocytes incubated under the indicated conditions for 6h (**D**) or in the presence or absence of the PPP inhibitor 6-aminonicotinamide (6-AN, **E**). β-Actin was used as a loading control. Shown is

one representative experiment out of 5. Bar charts depict quantification of Rac1 as ratio of non-prenylated Rac1 to prenylated Rac1 (n=5).

(**F** and **G**) Monocytes were transfected with IQGAP1 siRNA, and a control siRNA for 16h. (**F**) Representative Western blot shows siRNA mediated knockdown of *IQGAP1*. (**G**) Bar chart shows IL-1β release of transfected monocytes incubated under the indicated conditions for 8h (n=8). ATP and monosodium urate crystals (MSU) were used as controls (n=4).

(**H**) Overview of the hypothesized mechanism under glucose-oxygen deprivation.

Bars represent mean ± SD (A-C and E,G) or ± SEM (D), *$p < 0.05$, **$p < 0.01$, by Student's paired two-tailed t test (A –C and E, G), Mann-Whitney U test (D) Each dot represents a single biological replicate.

Supplementary Materials

Figs. S1-S10

Supplemental Figure 1

Supplemental Figure 1. Metabolites of glycolysis and tricarboxylic acid (TCA) cycle
Concentrations of intracellular glycolytic (A) and TCA cycle metabolites (B) were determined after extraction from monocytes incubated under the indicated conditions with methanol/chloroform and measured using IC-MS/MS. Peak areas were normalized to unstimulated freshly isolated cells. Shown are mean values of $n = 7$ (±SEM) experiments from three different donors.

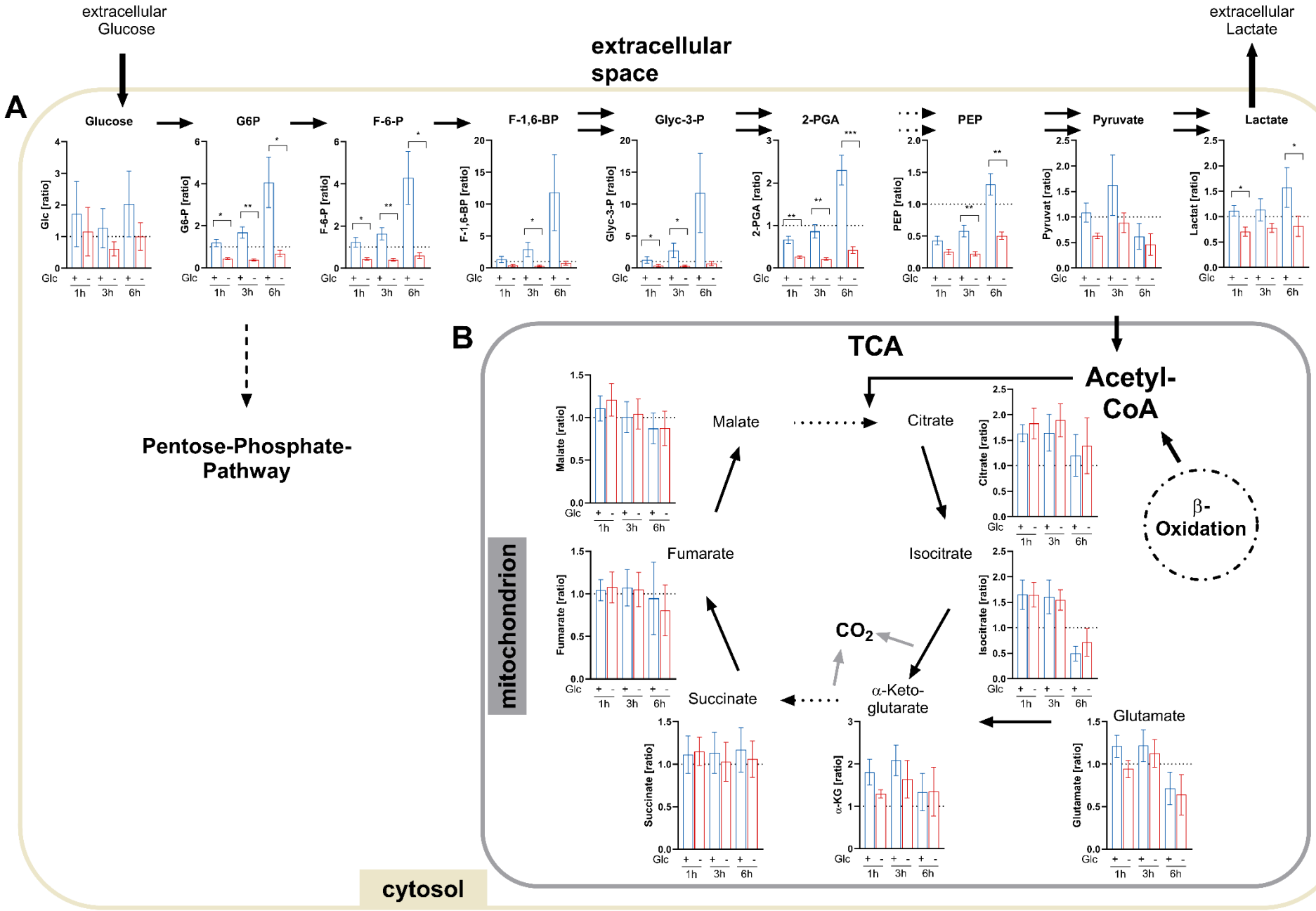
extracellular Glucose
extracellular space
extracellular Lactate
A
Glucose
G6P
F-6-P
F-1,6-BP
Glyc-3-P
2-PGA
PEP
Pyruvate
Lactate
Glc [ratio]
G6-P [ratio]
F-6-P [ratio]
F-1,6-BP [ratio]
Glyc-3-P [ratio]
2-PGA [ratio]
PEP [ratio]
Pyruvat [ratio]
Lactat [ratio]
Glc + - + - + -
1h 3h 6h
Pentose-Phosphate-Pathway
B
TCA
Acetyl-CoA
Malate
Citrate
Fumarate
Isocitrate
Succinate
α-Keto-glutarate
Glutamate
β-Oxidation
CO2
Malate [ratio]
Citrate [ratio]
Fumarate [ratio]
Isocitrate [ratio]
Succinate [ratio]
α-KG [ratio]
Glutamate [ratio]
mitochondrion
cytosol

Supplemental Figure 2

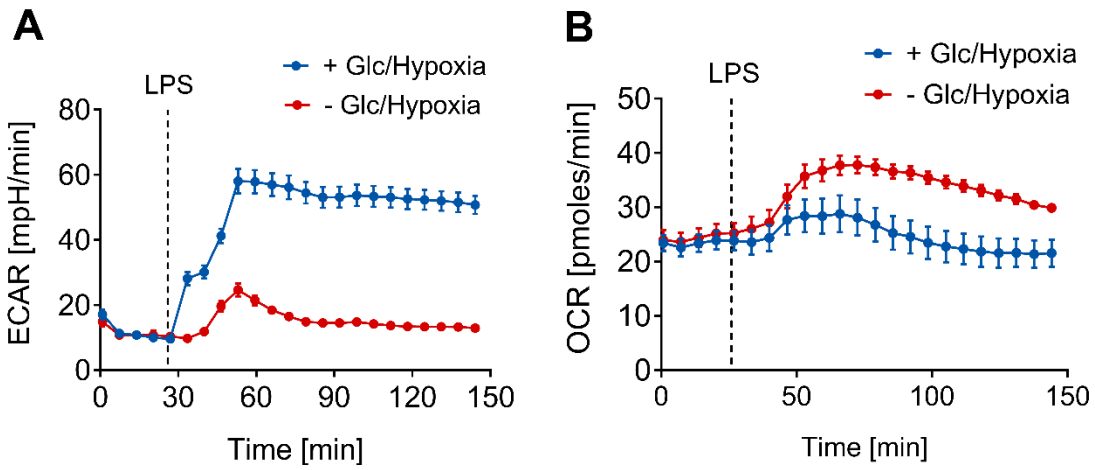

Supplemental Figure 2: Concomitant glucose and oxygen deprivation leads to increased oxidative phosphorylation to compensate for the energy demands of activated monocytes. Seahorse XF96 analyzer measurements of (A) extracellular acidification rate (ECAR) and (B) oxygen consumption rate (OCR) of LPS-stimulated monocytes (t=20min) under indicated conditions. Shown are means ± SEM from 6 donors.

Supplemental Figure 3

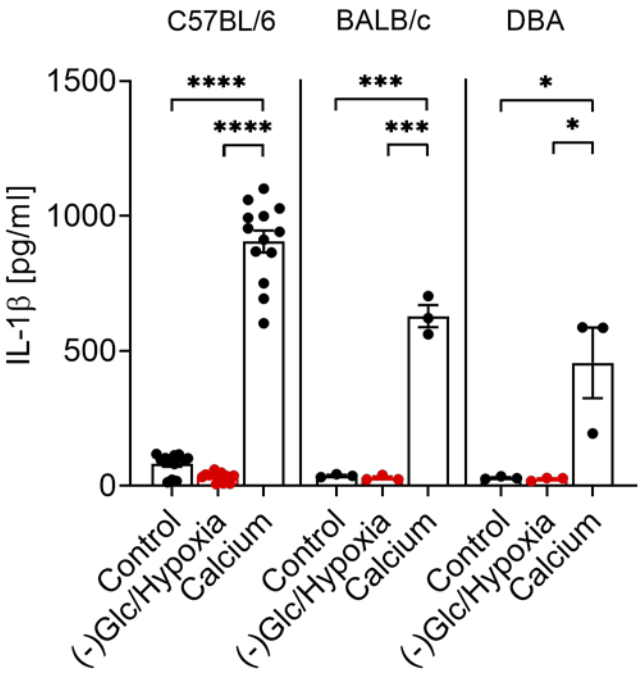

Supplemental Figure 3: Glucose-oxygen deprivation of mouse monocytes does not induce IL-1β release.
Bar chart depicts IL-1β release of LPS-primed peripheral blood monocytes from the three mouse strains indicated under glucose-oxygen deprivation ((-)Glc/Hypoxia) in comparison to standard conditions (Control) and stimulation with extra-cellular calcium ions (Calcium) for 16 h. n=13 for C57BL/6 and n=3 for BALB/c and DBA. Bars represent mean ± SEM, *p < 0.05, ***p < 0.001, ****p < 0.0001 by Student's unpaired two-tailed t test.

Supplemental Figure 4

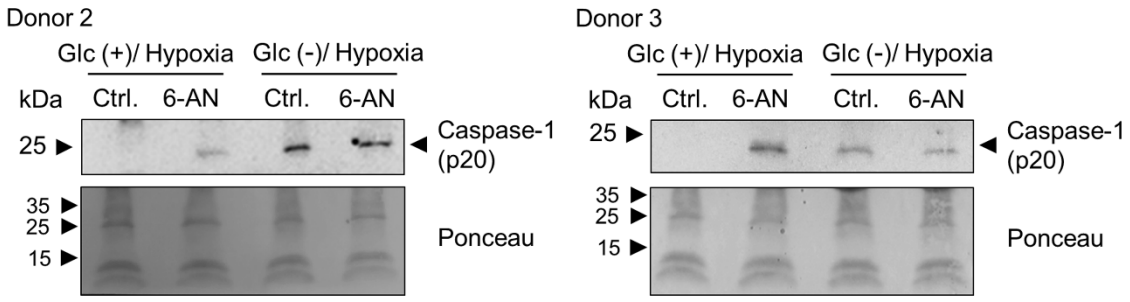

Supplemental Figure 4: Active caspase-1 after G6PD inhibition under Hypoxia
Western blot analysis of the supernatant of LPS-primed monocytes under indicated conditions after addition of glucose-6-phosphate dehydrogenase (G6PD) inhibitor 6-aminonicotinamide (6-AN, 50µM) for 16h (Fig. 2I). Ponceau staining was used as loading control. Shown are two representative experiments out of 3 with 3 donors.

Supplemental Figure 5

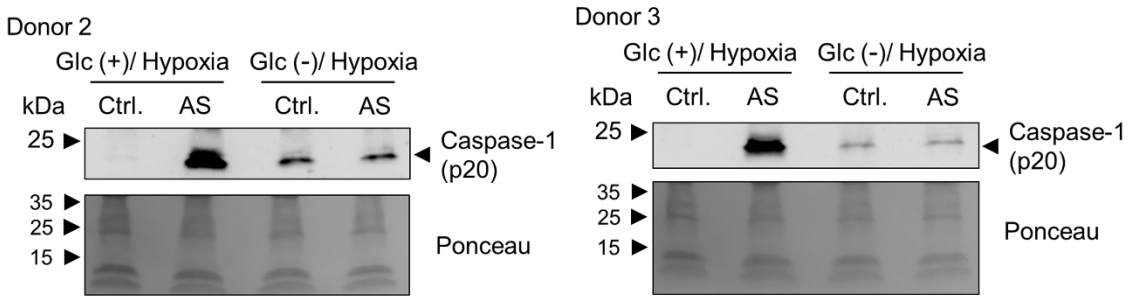

Supplemental Figure 5: **Active caspase-1 after HMGCR inhibition under Hypoxia**
Western blot analysis of the supernatant of LPS-primed monocytes under indicated conditions after addition of HMG CoA reductase (HMGCR) inhibitor atorvastatin (AS, 10μM) for 16h (Fig. 3C). Ponceau staining was used as loading control. Shown are two representative experiments out of 3 with 3 donors.

Supplemental Figure 6

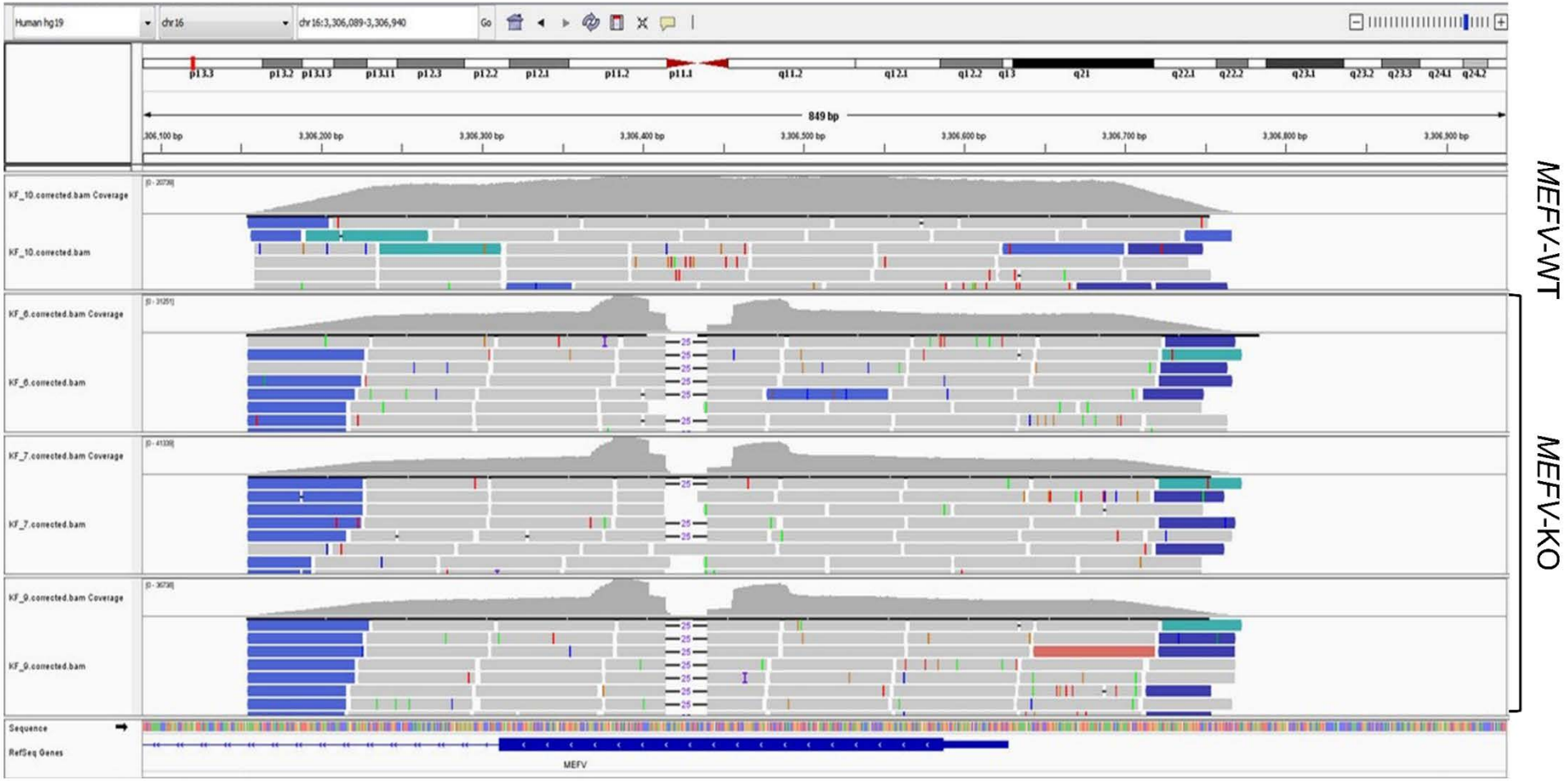

Supplemental Figure 6: Sequencing results and coverage of THP-1 *MEFV* knockout (KO) clones compared to wild type (WT).
Sequencing (n=4) shows that all THP-1 *MEFV*-KO clones (6, 7, 9) contain a 25 bp deletion at the edited sites.

Supplemental Figure 7

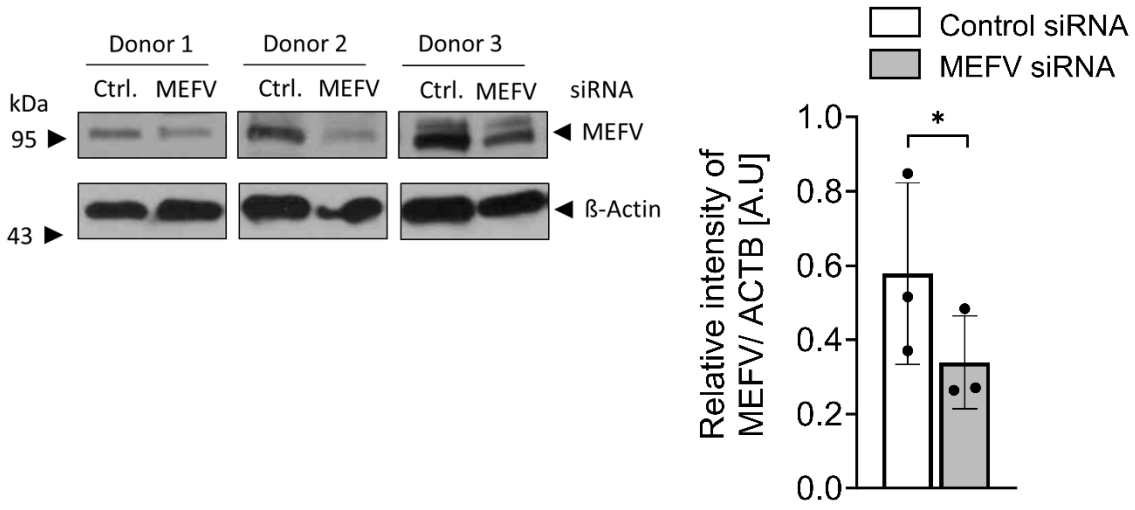

Supplemental Figure 7: siRNA-mediated *MEFV* knock down in monocytes
Western blot analysis of protein expression (left) and quantification (right) of monocytes transfected with siRNA specific for pyrin (*MEFV*) and a control siRNA for 16 hours. ß-Actin was used as loading control (Fig. 5C). Shown are three representative experiments out of 3 with 3 donors. Bars represent mean of ± SD, *p < 0.05, ***p < 0.001, ****p < 0.0001 by ratio paired t-test.

Supplemental Figure 8

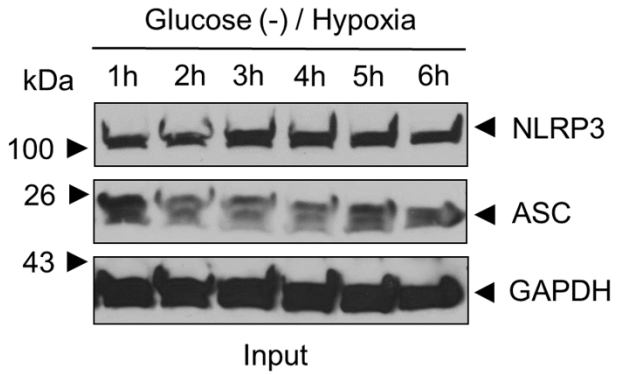

Supplemental Figure 8: Input controls
Input controls of immune precipitation of NLRP3 (Fig. 5F) in lysates of monocytes incubated under glucose-oxygen deprivation at the indicated time points. Shown is one representative experiment out of 3 with 2 donors.

Supplemental Figure 9

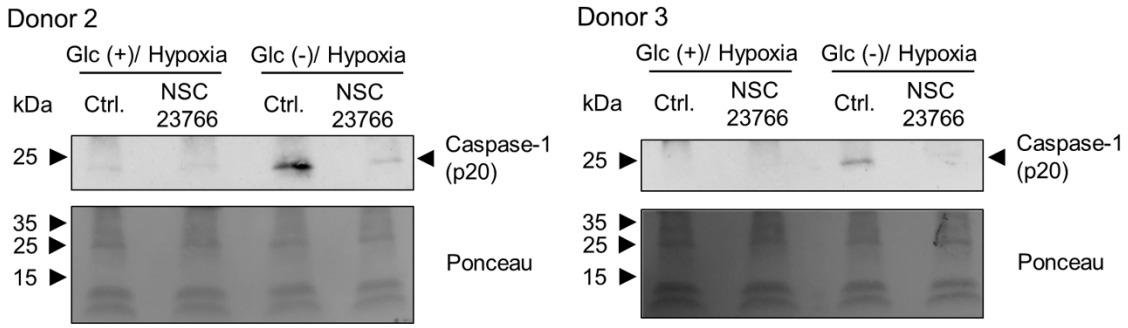

Supplemental Figure 9: Glucose-oxygen deprivation activates Rac1 and mediates caspase-1 activation

Western blot analysis of the supernatant of LPS-primed monocytes under indicated conditions after addition of the Rac1 inhibitor NSC 23766 (10µM) for 16h (Fig. 6B). Ponceau staining was used as loading control. Shown are two representative experiments out of 3 with 3 donors.

Supplemental Figure 10

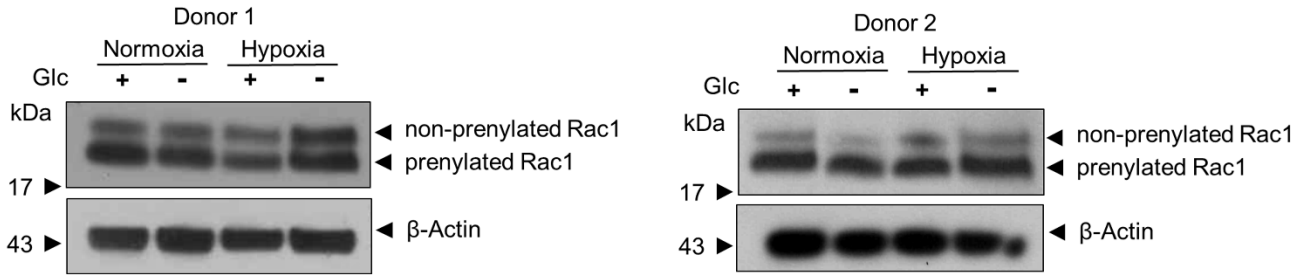

Supplemental Figure 10: Hypoxia increased fraction of non-prenylated Rac1 in MKD patients
Western blot analysis of the prenylation status of Rac1 in lysates of monocytes from 2 adult patients with mevalonate kinase deficiency (MKD) under the indicated conditions for 16h. ß-Actin was used as loading control. Shown are two representative experiments out of 2 from 2 donors.